J. Fluid Mech. (2014), *vol.* 738, *pp.* 34–64. © Cambridge University Press 2013
doi:10.1017/jfm.2013.579

Transient ventilation dynamics induced by heat sources of unequal strength

Ajay B. Shrinivas[1] **and Gary R. Hunt**[2,†]

[1]Department of Civil and Environmental Engineering, Imperial College London, London SW7 2AZ, UK
[2]Department of Engineering, University of Cambridge, Trumpington Street, Cambridge CB2 1PZ, UK

(Received 22 March 2013; revised 14 October 2013; accepted 29 October 2013;
first published online 2 December 2013)

We examine theoretically the transient displacement flow and density stratification that develops within a ventilated box after two localized floor-level heat sources of unequal strengths are activated. The heat input is represented by two non-interacting turbulent axisymmetric plumes of constant buoyancy fluxes B_1 and $B_2 > B_1$. The box connects to an unbounded quiescent external environment of uniform density via openings at the top and base. A theoretical model is developed to predict the time evolution of the dimensionless depths λ_j and mean buoyancies δ_j of the 'intermediate' ($j = 1$) and 'top' ($j = 2$) layers leading to steady state. The flow behaviour is classified in terms of a stratification parameter $\mathcal{S}$, a dimensionless measure of the relative forcing strengths of the two buoyant layers that drive the flow. We find that $\mathrm{d}\delta_1/\mathrm{d}\tau \propto 1/\lambda_1$ and $\mathrm{d}\delta_2/\mathrm{d}\tau \propto 1/\lambda_2$, where τ is a dimensionless time. When $\mathcal{S} \ll 1$, the intermediate layer is shallow (small λ_1), whereas the top layer is relatively deep (large λ_2) and, in this limit, δ_1 and δ_2 evolve on two characteristically different time scales. This produces a time lag and gives rise to a 'thermal overshoot', during which δ_1 exceeds its steady value and attains a maximum during the transients; a flow feature we refer to, in the context of a ventilated room, as 'localized overheating'. For a given source strength ratio $\psi = B_1/B_2$, we show that thermal overshoots are realized for dimensionless opening areas $A < A_{oh}$ and are strongly dependent on the time history of the flow. We establish the region of $\{A, \psi\}$ space where rapid development of δ_1 results in $\delta_1 > \delta_2$, giving rise to a bulk overturning of the buoyant layers. Finally, some implications of these results, specifically to the ventilation of a room, are discussed.

Key words: convection, plumes/thermals, stratified flows

1. Introduction

The 'filling-box' and 'emptying filling-box' problems have received considerable attention in the last two decades, not least because the simplified models capture key features of heat accumulation and airflow dynamics within buildings, relevant to aiding and guiding the efficient design of naturally ventilated spaces. The models provide architects and engineers with a means of predicting the internal thermal stratification resulting from active heat sources and the rate at which warm air is passively purged via ventilation openings due to a net vertical flow driven by

† Email address for correspondence: gary.hunt@eng.cam.ac.uk

https://doi.org/10.1017/jfm.2013.579 Published online by Cambridge University Press

the naturally occurring forces of wind and buoyancy. Currently, energy expenditure attributed to cooling modern commercial buildings using mechanical ventilation and air-conditioning accounts for more than 50 % of their total electricity consumption (Wagner, Klebe & Parker 2007). Considerable efforts to better understand building airflows have been fuelled by the potentially significant energy savings inherent in the use of natural ventilation and the need to address environmental objectives on reducing carbon emissions. Filling-box models have also offered considerable insight in other contexts, for example in oceanographic applications (Hughes & Griffiths 2008).

The present work considers the transient airflow dynamics within a ventilated enclosure induced by two heat sources of unequal strength. In particular, we examine the response of an emptying filling-box system to the simultaneous activation of both heat sources in an initially unstratified environment, which gives rise to the classical transition from an unheated room to a heated room. We also consider a steady two-layer stratification first established by the activation of a single heat source and investigate the transient dynamics resulting from the activation of a second, stronger or weaker, source. This investigation addresses two pertinent issues. First, in contrast to previous studies, the transients as a buoyancy-driven ventilation flow adjusts between two characteristically different steady states have received little attention. The problem has considerable practical significance as interior airflows typically vary over a diurnal cycle due to changing patterns in occupancy and use of electrical equipment at specific times. Secondly, in practice, the strengths of heat sources within buildings may vary by at least an order of magnitude and range from relatively weak (for example occupants and lighting) to relatively strong (for example computers and heaters). Herein, we develop a theoretical model to predict the time-dependent stratification established by two localized buoyancy sources of unequal strength at floor-level and show that the difference in forcing strengths can give rise to thermal discomfort for room occupants for a significant duration of the transients, despite comfortable conditions at steady state.

Baines & Turner (1969) conducted the first fundamental investigation of buoyancy-driven flows within a closed box and developed a mathematical model to predict the time-dependent stratification resulting from the continuous supply of buoyancy from a localized source producing a turbulent plume. Wong & Griffiths (1999) generalized this filling-box model to account for multiple non-interacting sources of unequal strength.

If the box is connected to a quiescent external environment of uniform density via openings at the top and base, Kaye & Hunt (2004) showed that the density stratification which develops internally is governed by the time-dependent balance between the 'filling' flow attributed to the supply of buoyant fluid from rising turbulent plumes and a 'draining' flow responsible for purging warm air through the top opening(s). A single plume or multiple (non-interacting) plumes of equal strength produce a deepening buoyant upper layer, separated from the layer at ambient density below by an interface that is continuously sharpened by entrainment into the plume(s).

When the filling and draining flows are balanced, the flow subsequently reaches a steady state in which the buoyant upper layer is of uniform density. The steady flow theory of Linden, Lane-Serff & Smeed (1990) shows that the dimensionless interface height $\xi_{ss} = h_{ss}/H$ (the subscript 'ss' denoting steady state), in a box of height H, is independent of the source strength and satisfies

$$\frac{A^*}{nC^{3/2}H^2} = \left(\frac{\xi_{ss}^5}{1-\xi_{ss}}\right)^{1/2}, \quad C = \frac{6\alpha}{5}\left(\frac{9\alpha\pi^2}{10}\right)^{1/3}, \tag{1.1}$$

https://doi.org/10.1017/jfm.2013.579 Published online by Cambridge University Press

where α is the 'top-hat' entrainment coefficient for an axisymmetric turbulent plume, n is the number of localized heat sources and A^* is an 'effective' vent area, which Kaye & Hunt (2004) express as

$$\frac{1}{A^{*2}} = \frac{1}{2c_b^2 a_b^2} + \frac{1}{2c_t^2 a_t^2}, \tag{1.2}$$

for openings at the top and base of areas a_t and a_b, respectively. The quantities c_b and c_t are dimensionless coefficients that account for flow contraction and dissipative losses associated with the inlet and outlet openings.

Kaye & Hunt (2004) identified that following the (simultaneous) activation of one or more identical sources, the interface may descend below the steady height resulting in an 'overshoot'. Subsequent studies on transient ventilation flows that have considered an instantaneous change in source strength (Bower *et al.* 2008), time-varying sources (Economidou & Hunt 2010) and effects of an opposing wind (Coomaraswamy & Caulfield 2011) have also demonstrated that the buoyant upper layer may overshoot its steady depth.

Cooper & Linden (1996) showed that the steady flow established by two plumes of unequal strengths B_1 and $B_2 > B_1$ is characterized by a three-layer stratification (top, intermediate and lower layers) as depicted in the right-hand column of figure 1. They showed that the two steady interface positions ($\xi_{1,ss} = h_{1,ss}/H$, $\xi_{2,ss} = h_{2,ss}/H$) are dependent only on the dimensionless area $A^*/(C^{3/2}H^2)$ and the buoyancy flux ratio $\psi = B_1/B_2$. Inherent in this problem is the influence of the intermediate layer on plume behaviour. First, the stronger plume (source strength B_2) experiences a reduction in buoyancy flux at the lower interface due to the density change in the environment. Secondly, the weaker plume rises within the intermediate layer as a dense fountain and provided its rise height exceeds the (intermediate) layer depth, it impinges on the upper interface and turbulently entrains, downwards, a volume flux Q_e from the top layer. Although it is possible to account for the reduction in B_2 and the entrainment flux Q_e, Linden & Cooper (1996) showed that in their absence, the analytic solution

$$\frac{A^*}{C^{3/2}H^2} = \frac{\xi_{2,ss}^{5/2}}{[1 - \xi_{2,ss}(1 - \hat{g}') - \xi_{1,ss}\hat{g}']^{1/2}}, \tag{1.3}$$

$$\left(\frac{\xi_{2,ss}}{\xi_{1,ss}}\right)^{5/3} = \frac{1 + \psi^{1/3}}{(1 + \psi)^{1/3}}, \quad \hat{g}' = \frac{g'_{1,ss}}{g'_{2,ss}} = \frac{\psi^{2/3}(1 + \psi^{1/3})}{1 + \psi}, \tag{1.4}$$

provides an accurate prediction of the lower interface position $\xi_{1,ss}$ for $\psi > 0$ and a reasonably good prediction of the upper interface position $\xi_{2,ss}$ for $0 < \psi < 0.4$. In (1.3) and (1.4), the buoyancy of layer j $(= 1, 2)$ is denoted $g'_{j,ss} = g(\rho - \rho_{j,ss})/\rho$, where ρ is the density of the external ambient and $\rho_{j,ss}$ is the steady density of layer j.

Whilst the steady displacement flow driven by two unequal plumes is well understood through the work of Cooper & Linden (1996), we raise the question of what happens to the layer depths and their buoyancies in the lead up to this equilibrium state. Our aim is to examine the time evolution of the stratification within a ventilated box that is subject to a continuous input of buoyancy flux from two localized sources of unequal strength. In § 2, by neglecting the reduction in B_2 and the entrainment flux Q_e, we develop a simplified theoretical model that predicts the interior stratification and the volume flux through the box leading to steady state. We analyse the model predictions in § 3 and present a theory on thermal overshoots that elucidates the reasons why the mean buoyancy of the intermediate layer exceeds its steady value during the transients and attains a maximum before relaxing back to its

https://doi.org/10.1017/jfm.2013.579 Published online by Cambridge University Press

equilibrium state. Physical arguments are provided for two other key flow features identified by our model, namely, the overshoot of the lower density interface and the bulk overturning of the buoyant layers. Implications for the heating of a room are discussed and conclusions are drawn in § 4. Furthermore, time-dependent models for the system that account for the reduction in B_2 and the entrainment flux Q_e are presented in the Appendix. By comparing their predictions with those of the simplified model, we show that the transient dynamics are typically little affected by the change in the stronger plume's buoyancy flux and the fountain–interface interaction.

2. A theoretical model for unequal plumes in a ventilated box

We examine the time-dependent buoyancy-driven flow induced by two continuous, floor-level ($z = 0$) sources of unequal strength that give rise to turbulent, Boussinesq, non-interacting, axisymmetric pure plumes of constant source buoyancy flux B_1 and $B_2 > B_1$. The finite region of interest is a box of internal height H and horizontal cross-sectional area S (independent of H) that connects to an unbounded stationary ambient of constant, uniform density ρ via openings of area a_t at the top and a_b at the base. Following Cooper & Linden (1996) we postulate that the unequal plumes establish a three-layer stratification comprised of two buoyant layers and a lower region at ambient density.

The stratification may develop in several distinct ways depending on the sequence in which the sources are activated. Initiating both sources simultaneously at $t = 0$ when the interior is at ambient density, gives rise to what we shall refer to as a 'filling' flow. Initially, fluid from both plumes ascends to the top of the box and their outflows spread laterally as gravity currents, subsequent to which, the stronger plume's outflow rises over that of the weaker plume to establish a stable stratification (Wong & Griffiths 1999). The two interfaces formed descend as the buoyant layers deepen, *filling* the box; see figure 1(*a*).

If, instead, a localized source of strength B_2 has established a steady two-layer stratification with an interface at a height $z = h_{10}$, activation at $t = 0$ of a weaker source, of buoyancy flux $B_1 < B_2$, introduces a second turbulent plume that is cooler at all heights above the source. Initially, the upper layer is uniform and of a density equal to that in the strong plume at the height of the interface. Consequently, upon penetrating the interface, the weaker plume becomes negatively buoyant and its upward motion is terminated. The outflow from this weaker plume spreads laterally along the interface at $z = h_{10}$ to form an intermediate layer which is fed with increasingly buoyant fluid as the original (i.e. lowermost) interface descends. The intermediate and top layers are separated by the newly formed interface at height $z = h_2(t)$. The stronger plume rises through both interfaces and discharges fluid continuously into the top layer. Two mechanisms contribute to the top layer's depletion: turbulent entrainment by the weaker plume (see § A.2) and fluid vented out via the top opening(s). As the flow evolves, the new interface ascends and therefore, we refer to flows of this type as 'ascending' flows; see figure 1(*b*).

If, in contrast, a steady two-layer flow is first established by the weaker plume, activation at $t = 0$ of a second, stronger buoyancy source gives rise to a turbulent plume that, on reaching the interface at height $z = h_{10}$, is positively buoyant relative to the original upper layer. Therefore, the stronger plume forms a new layer at the top of the box with a density interface, established at height $h_2(t)$, separating the now intermediate layer and new top layer. As the flow evolves, both interfaces descend and hence, we refer to flows of this type as 'descending' flows; see figure 1(*c*).

https://doi.org/10.1017/jfm.2013.579 Published online by Cambridge University Press

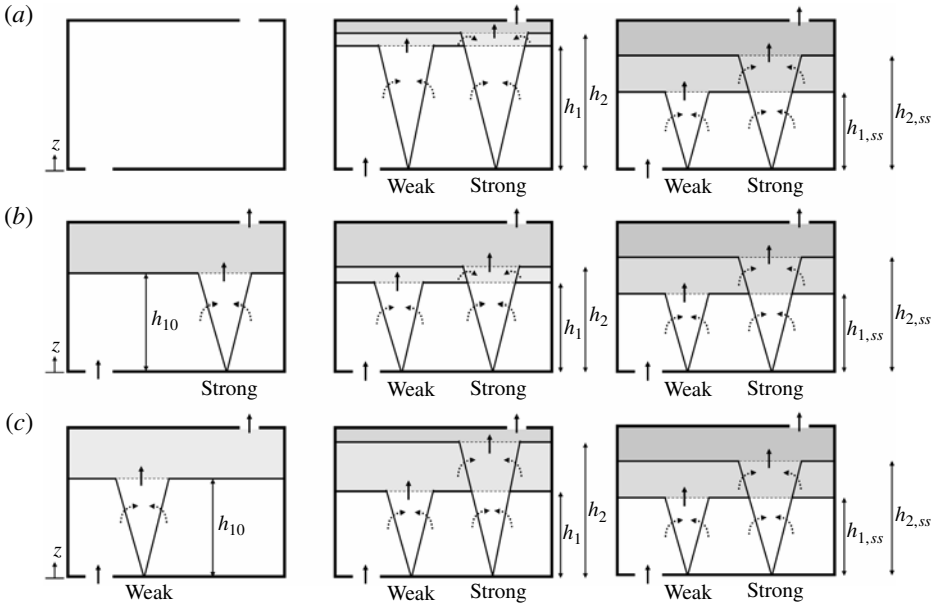


FIGURE 1. Schematics show 'filling' (*a*), 'ascending' (*b*) and 'descending' (*c*) flows established by buoyancy sources of unequal strength (labelled as 'weak' and 'strong'). The left-hand column illustrates the three initial states, the centre column an instant during the transients, and the right-hand column the steady state. Solid arrows indicate bulk flow direction and dotted arrows indicate plume entrainment.

A key feature of all three flows (filling, ascending and descending) is that bulk fluid transport across the two interfaces only occurs as a result of turbulent entrainment by the plumes/fountain. All three layers are assumed to be well-mixed and of uniform density at each time instant and, therefore, instantaneous mean buoyancies,

$$g_1'(t) = g\left(\frac{\rho - \rho_1(t)}{\rho}\right), \quad g_2'(t) = g\left(\frac{\rho - \rho_2(t)}{\rho}\right), \tag{2.1}$$

are assigned to layers 1 and 2, respectively, figure 2. The uniform layer assumption implies that the plume supplying a given buoyant layer induces instantaneous and 'complete' mixing of the fluid within the layer, thus producing a uniform distribution of buoyancy over the layer depth. As noted by Coomaraswamy & Caulfield (2011), this is a reasonable assumption when the time scale for the mixing (driven by the plume) is small compared with the time scale for the development of the layer thickness. Previous studies have shown that theoretical predictions are typically in good agreement with experimental results when the uniform layer assumption is adopted (see Kaye & Hunt 2004; Flynn & Caulfield 2006; Bower *et al.* 2008 for a detailed discussion). Nevertheless, it is an idealization and we expect the stratification within layers 1 and 2 to be closer to that of a filling-box (Baines & Turner 1969) during the early transients. Conceptually, one may regard the well-mixed buoyant layers modelled as regions within the box where the fluid motion predominantly originates from, and is dominated by, an individual plume; the top layer bounds the region in which the flow is primarily controlled by the stronger plume and the intermediate layer characterizes the vertical extent over which the flow is primarily controlled by the weaker plume.

https://doi.org/10.1017/jfm.2013.579 Published online by Cambridge University Press

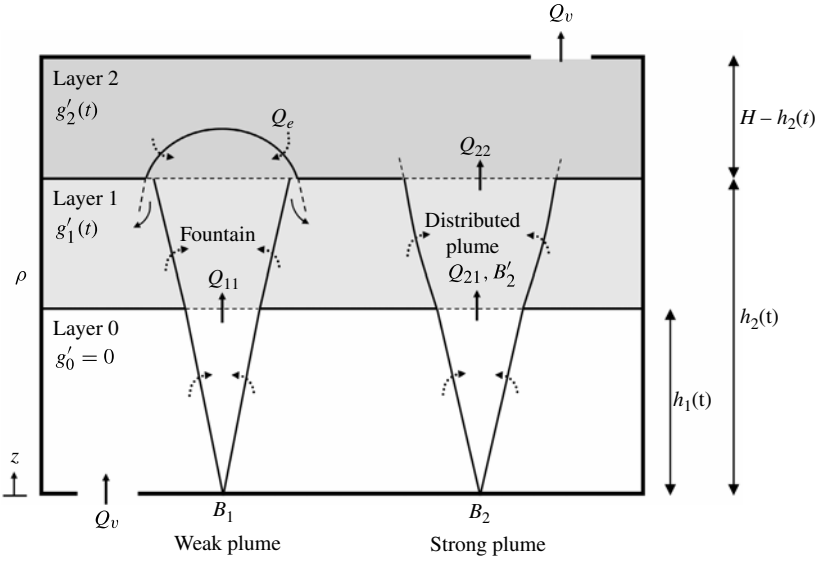


FIGURE 2. Schematic of a ventilated box with two non-interacting localized buoyancy sources of unequal strength ($B_1 < B_2$) at $z = 0$, showing nomenclature and the basic three-layer stratification at some time after activation of the sources at $t = 0$. Beginning at the base of the box and moving upwards, the layers are numbered 0, 1 and 2.

The equations governing the two interface positions (h_1, h_2) and mean buoyancies (g_1', g_2') are developed for a generic three-layer displacement flow (figure 2) and the three flow types are defined by three unique sets of initial conditions. Typically, one expects the outflow thicknesses of the strong and weak plumes, b_s and b_w, respectively, to be non-zero. Wong & Griffiths (1999) found that $0.2 \lesssim b_s/H \lesssim 0.25$, whereas shear layers generated by the stronger plume outflow influenced the spreading of the weaker plume outflow and, hence, estimates of b_w were not reported. We ignore the details of the laterally spreading gravity currents and plume–outflow interaction and for simplicity apply the classical filling-box assumption of Baines & Turner (1969), namely that an infinitesimally thin layer forms, as a consequence of the source activated, at $t = 0$. As we will see (e.g. figure 3), the layer depths develop rapidly (certainly at rates greater than the mean buoyancies), exceeding the expected finite outflow thicknesses (Wong & Griffiths 1999) early in the transients and typically within fractions of a Baines & Turner (1969) filling-box time scale (see (2.21)). Whilst the formation of strong horizontal shear layers resulting from the plume outflow may have an influence on the early transients (Wong, Griffiths & Hughes 2001) we neglect their effects here.

Overturning of the plume outflow, caused by its impingement on the side boundaries, is neglected and this places restrictions on the aspect ratio H/W of the box, where W is the box width. Following Barnett (1991) and Kaye & Hunt (2007), we limit our attention to $H/W \lesssim 1$. Furthermore, we assume that there are no buoyancy exchanges with the side boundaries or with the upper and lower boundaries as considered by Holford & Woods (2007) and Lane-Serff & Sandbach (2012).

We assume that the flow remains uni-directional (i.e. in through the base opening and out through the top opening) and that there is no interfacial mixing caused by the inflowing jet of ambient fluid, via the base opening(s), impinging on the lower

https://doi.org/10.1017/jfm.2013.579 Published online by Cambridge University Press

interface. Hunt & Coffey (2010) showed that two Froude numbers, Fr_b and Fr_t, associated with the flows through the base and top openings, determine the vigour of interfacial mixing and flow direction. To achieve a (classical) displacement flow in the absence of mixing, $Fr_b < 0.67$ and $Fr_t > 0.33$. This places formal restrictions on a_t/H^2 and a_b/H^2, which are given in Hunt & Coffey (2010).

Besides the geometry, also controlling the flow within the box are the two turbulent plumes, the dynamics of which are influenced by the intermediate layer. The stronger plume's buoyancy flux reduces from B_2 to B_2' due to the density change in the environment at $z = h_1$. Fluid from the weaker plume rises within layer 1 as a dense fountain and provided its rise height exceeds the depth of layer 1 $(h_2 - h_1)$, it impinges on the upper interface and turbulently entrains a volume flux Q_e from layer 2. However, following Linden & Cooper (1996), we first ignore the aforementioned effects and develop a theoretical model assuming that the source buoyancy flux of the stronger plume is unchanged as it rises up to a height h_2 (so that $B_2' = B_2$) and that $Q_e = 0$. These two simplifications greatly aid the analysis of the flow behaviour and provide a convenient means of fully comprehending the rich dynamics. In §§ A.1 and A.2, we extend our model and incorporate the stronger plume behaviour within layer 1 and the turbulent entrainment across the upper interface. We show that, in general, these features only have a minor effect on the layer depths and mean buoyancies.

Assuming an incompressible flow, conservation of volume for layer 2 requires

$$\frac{\mathrm{d}}{\mathrm{d}t}[S(H - h_2)] = Q_{22} - Q_v, \tag{2.2}$$

where Q_v denotes the volume flux through the box (figure 2) and Q_{22} the volume flux in plume 2 at the height of interface 2. The stronger plume entrains a volume flux $(Q_{22} - Q_{21})$ from layer 1 between heights $h_1(t)$ and $h_2(t)$. Therefore, conservation of volume for layer 1 requires

$$\frac{\mathrm{d}}{\mathrm{d}t}[S(h_2 - h_1)] = Q_{11} - (Q_{22} - Q_{21}). \tag{2.3}$$

Substituting for $\mathrm{d}h_2/\mathrm{d}t$ from (2.2), the time rate of change of h_1 is, from (2.3),

$$\frac{\mathrm{d}h_1}{\mathrm{d}t} = \frac{Q_v - Q_{11} - Q_{21}}{S}. \tag{2.4}$$

Conservation of buoyancy for layer 2 requires

$$\frac{\mathrm{d}}{\mathrm{d}t}[Sg_2'(H - h_2)] = B_{in,2} - B_{out,2}, \tag{2.5}$$

where $B_{out,2} = Q_v g_2'$ is the flux of buoyancy expelled through the top opening and $B_{in,2}$, which denotes the buoyancy flux supplied to layer 2, is comprised of (*a*) the stronger plume's source buoyancy flux B_2 and (*b*) the flux of buoyancy $g_1'(Q_{22} - Q_{21})$ entrained from layer 1 by the stronger plume, so that $B_{in,2} = B_2 + g_1'(Q_{22} - Q_{21})$. Introducing these expressions for $B_{in,2}$ and $B_{out,2}$ in (2.5), gives the time rate of change of g_2':

$$\frac{\mathrm{d}g_2'}{\mathrm{d}t} = \frac{B_2 + g_1'(Q_{22} - Q_{21}) - g_2'Q_{22}}{S(H - h_2)}. \tag{2.6}$$

Similar buoyancy conservation arguments for layer 1 give

$$\frac{\mathrm{d}}{\mathrm{d}t}[Sg_1'(h_2 - h_1)] = B_{in,1} - B_{out,1}, \tag{2.7}$$

https://doi.org/10.1017/jfm.2013.579 Published online by Cambridge University Press

where $B_{in,1} = Q_{11}G'_{11}$ is the flux of buoyancy supplied by the weaker plume at $z = h_1$ and $B_{out,1} = g'_1(Q_{22} - Q_{21})$ is the buoyancy flux removed by the stronger plume. Here G'_{11} denotes the mean buoyancy of the weaker plume at $z = h_1$. Substituting for $B_{in,1}$ and $B_{out,1}$, and for $\mathrm{d}h_1/\mathrm{d}t$ and $\mathrm{d}h_2/\mathrm{d}t$ from (2.4) and (2.2), the time rate of change of g'_1 is

$$\frac{\mathrm{d}g'_1}{\mathrm{d}t} = \frac{B_1 - Q_{11}g'_1}{S(h_2 - h_1)}. \tag{2.8}$$

To close the problem, we require expressions for the volume fluxes within the plumes (Q_{11}, Q_{21} and Q_{22}) and the volume flux through the box (Q_v). For self-similar, pure turbulent plumes their time-averaged volume fluxes at $z = h_1$ can be expressed (Morton, Taylor & Turner 1956) as

$$Q_{11} = CB_1^{1/3}h_1^{5/3}, \quad Q_{21} = CB_2^{1/3}h_1^{5/3}. \tag{2.9}$$

For Gaussian profiles, Turner (1986) suggested that an entrainment constant $\alpha_G = 0.083$ is a suitable empirical value. For top-hat profiles, we have $\alpha = \sqrt{2}\alpha_G \approx 0.117$ and hence from (1.1), $C \approx 0.14$. To quantify Q_{22}, we invoke the assumption that the source buoyancy flux B_2 of the stronger plume is unchanged as it rises through layers 0 and 1. Accordingly, at the height of the upper interface $z = h_2$, the buoyancy flux within the strong plume is comprised of the source buoyancy flux B_2 and the flux of non-zero buoyancy $g'_1(Q_{22} - Q_{21})$ entrained from layer 1 over the height $(h_2 - h_1)$, i.e. $B_{22} = B_2 + g'_1(Q_{22} - Q_{21})$. Thus, from plume theory,

$$Q_{22} = CB_{22}^{1/3}h_2^{5/3} = C[B_2 + g'_1(Q_{22} - Q_{21})]^{1/3}h_2^{5/3}. \tag{2.10}$$

Evidently, Q_{22} depends on B_2 and the buoyancy flux entrained from layer 1 (the second term in the parenthesis of (2.10)). This forms an implicit expression which can be rewritten as a cubic in Q_{22}:

$$Q_{22}^3 - (C^3h_2^5g'_1)Q_{22} + C^3h_2^5(g'_1Q_{21} - B_2) = 0. \tag{2.11}$$

The cubic has only one positive root and, hence, there exists only one physical solution for Q_{22} for $t > 0$. In the Appendix, we use classical plume theory of Morton *et al.* (1956) to analyse the stronger plume within layer 1 and account for the reduction in B_2 to estimate Q_{22}. Following Cooper & Linden (1996), the volume flux through the openings

$$Q_v = A^*\left(\int_0^H g'(z,t)\,\mathrm{d}z\right)^{1/2} = A^*\sqrt{g'_1(h_2 - h_1) + g'_2(H - h_2)}. \tag{2.12}$$

At this stage, it is convenient to non-dimensionalize the governing equations: interface heights are scaled on H, layer buoyancies on the buoyancy within the stronger plume at $z = H$ in an environment of density ρ, and A^* on the square of H and the entrainment constant C:

$$\left.\begin{aligned} \xi_1 &= \frac{h_1}{H}, \quad \xi_2 = \frac{h_2}{H}, \quad \delta_1 = \frac{g'_1}{B_2^{2/3}C^{-1}H^{-5/3}}, \\ \delta_2 &= \frac{g'_2}{B_2^{2/3}C^{-1}H^{-5/3}}, \quad A = \frac{A^*}{C^{3/2}H^2}. \end{aligned}\right\} \tag{2.13}$$

We note that $A = 0$ corresponds to the unventilated filling-box scenario considered by Wong & Griffiths (1999) in which the top and bottom vents are closed, i.e. $a_t = a_b = 0$.

https://doi.org/10.1017/jfm.2013.579 Published online by Cambridge University Press

We scale the volume fluxes of interest on the volume flux within the stronger plume at $z = H$ in an environment of density ρ:

$$q_{11} = \frac{Q_{11}}{CB_2^{1/3}H^{5/3}} = \psi^{1/3}\xi_1^{5/3}, \quad q_{21} = \frac{Q_{21}}{CB_2^{1/3}H^{5/3}} = \xi_1^{5/3}, \quad q_v = \frac{Q_v}{CB_2^{1/3}H^{5/3}}. \tag{2.14}$$

The cubic in Q_{22}, (2.11), reduces to

$$q_{22}^3 - (\delta_1\xi_2^5)q_{22} + \xi_2^5(\delta_1\xi_1^{5/3} - 1) = 0, \tag{2.15}$$

and the dimensionless volume flux through the openings to

$$q_v = A\sqrt{\delta_1(\xi_2 - \xi_1) + \delta_2(1 - \xi_2)}. \tag{2.16}$$

When examining the time evolution of the stratification, it is informative to consider (*a*) the non-dimensional thicknesses of the buoyant layers so that for layers 1 and 2, respectively,

$$\lambda_1 = \xi_2 - \xi_1, \quad \lambda_2 = 1 - \xi_2, \tag{2.17}$$

and (*b*) the integral of the buoyancy of each layer over its depth,

$$\Delta_1 = \frac{CH^{2/3}}{B_2^{2/3}}\int_{h_1}^{h_2} g'(z,t)\,\mathrm{d}z = \lambda_1\delta_1, \quad \Delta_2 = \frac{CH^{2/3}}{B_2^{2/3}}\int_{h_2}^{H} g'(z,t)\,\mathrm{d}z = \lambda_2\delta_2. \tag{2.18}$$

In other words, Δ_1 and Δ_2 give the (non-dimensional) net buoyancy per unit cross-sectional area of each layer. Therefore, the net buoyancy within the box (per unit cross-sectional area) is

$$\Delta_N = \Delta_1 + \Delta_2. \tag{2.19}$$

For convenience, we herein refer to Δ_1, Δ_2 and Δ_N as 'net buoyancies' and note that $q_v = A\Delta_N^{1/2}$.

Hunt & Linden (2001) showed that the relative strengths of two forces (e.g. buoyancy and wind) driving a displacement flow may be characterized by the relative magnitudes of the fluid velocities they induce within the box. Accordingly, we introduce a ratio, $\mathcal{S}$, of the characteristic buoyancy-induced velocity of layer 1 ($\sqrt{\Delta_1}$) to the buoyancy-induced velocity of layer 2 ($\sqrt{\Delta_2}$), namely

$$\mathcal{S} = \sqrt{\frac{\Delta_1}{\Delta_2}}, \tag{2.20}$$

to characterize the relative contributions of the two buoyant layers in driving the overall flow through the box. For $\mathcal{S} \ll 1$ buoyancy forces produced by layer 2 dominate the fluid motion, whereas for $\mathcal{S} \gg 1$, layer 1 produces the dominant forcing. We interpret $\mathcal{S}$ as a stratification parameter, which, as we shall see, provides a convenient means of classifying the dynamics.

We find that the time scales on the filling-box time scale T_f and introduce the dimensionless time

$$\tau = \frac{t}{T_f} \quad \text{where } T_f = \frac{S}{CB_2^{1/3}H^{2/3}}. \tag{2.21}$$

Here T_f is the characteristic time associated with the stronger plume filling the unventilated box of height H and cross-sectional area S.

https://doi.org/10.1017/jfm.2013.579 Published online by Cambridge University Press

The non-dimensional forms of the governing equations are now

$$\frac{\mathrm{d}\xi_1}{\mathrm{d}\tau} = A\Delta_N^{1/2} - (\psi^{1/3}+1)\xi_1^{5/3}, \quad \frac{\mathrm{d}\xi_2}{\mathrm{d}\tau} = A\Delta_N^{1/2} - q_{22}, \tag{2.22a,b}$$

$$\frac{\mathrm{d}\delta_1}{\mathrm{d}\tau} = \frac{\psi - \psi^{1/3}\delta_1\xi_1^{5/3}}{\lambda_1}, \quad \frac{\mathrm{d}\delta_2}{\mathrm{d}\tau} = \frac{1 + q_{22}(\delta_1-\delta_2) - \delta_1\xi_1^{5/3}}{\lambda_2}. \tag{2.23a,b}$$

2.1. *Initial conditions*

For filling flows, the initial conditions are

$$\xi_{10} = 1, \quad \xi_{20} = 1, \quad \delta_{10} = \psi^{2/3}, \quad \delta_{20} = 1. \tag{2.24}$$

For ascending flows:

$$\left.\begin{array}{l} \xi_{10}^5 + A^2\xi_{10} - A^2 = 0 \text{ (from (1.1))}, \quad \xi_{20} = \xi_{10}, \\ \delta_{10} = \psi^{2/3}\xi_{10}^{-5/3}, \quad \delta_{20} = \xi_{10}^{-5/3}. \end{array}\right\} \tag{2.25}$$

For descending flows, ξ_{10} and δ_{10} are given by (2.25) and

$$\xi_{20} = 1, \quad \delta_{20} = [1 + \delta_{10}(q_{22}(\tau=0) - \xi_{10}^{5/3})]^{2/3}. \tag{2.26}$$

3. Theoretical predictions and analysis of results

Solution of the governing equations, (2.22*a,b*) and (2.23*a,b*), subject to the initial conditions prescribed in § 2.1 for the three flow types, was achieved using a fourth-order Runge–Kutta finite-difference scheme.

The time-dependent behaviour of the two interfaces and mean layer buoyancies for a typical filling, ascending and descending flow are shown in figures 3, 4 and 5, respectively. As expected, at large times, our transient model predictions approach the steady solutions, (1.3) and (1.4), of Linden & Cooper (1996). For the values of A and ψ considered, $\delta_2 > \delta_1$ for $\tau \geqslant 0$ and, hence, the stratification remains stable. In § 3.7 we identify the region of $\{A, \psi\}$ space for which $\delta_2 < \delta_1$, resulting in a bulk overturning of the buoyant region.

Two features of interest associated with the stratification can be identified from figures 4(*a*) and 4(*b*). First is the overshoot of the lower interface, typically observed in transient ventilation flows (Hunt & Linden 1998; Kaye & Hunt 2004), in which $\xi_1 < \xi_{1,ss}$. As an aside, we note from the measurements of Hunt & Linden (1998) that the density profile in the buoyant layer is close to uniform before overshoot. Given that our interface overshoots first occur typically within a single filling-box time scale (2.21), the assumption of uniform layers (§ 2) is only expected to influence the very early transients. The second feature of interest is an overshoot in the mean buoyancy of layer 1, a previously unidentified phenomenon. We define this thermal overshoot as occurring when the intermediate layer buoyancy exceeds its steady value

$$\delta_1 > \delta_{1,ss}. \tag{3.1}$$

A thermal overshoot can have practical implications as, for example, occupants of ventilated rooms may then experience higher temperatures than designed for based on the predictions of a steady model, as is standard in practice. As this phenomenon is restricted to the intermediate layer, occupants would experience ‘localized overheating’. Attention is also drawn to the significant time duration (approximately three filling-box time scales in the example in figure 4*b*) for which $\delta_1 > \delta_{1,ss}$. Filling and

https://doi.org/10.1017/jfm.2013.579 Published online by Cambridge University Press

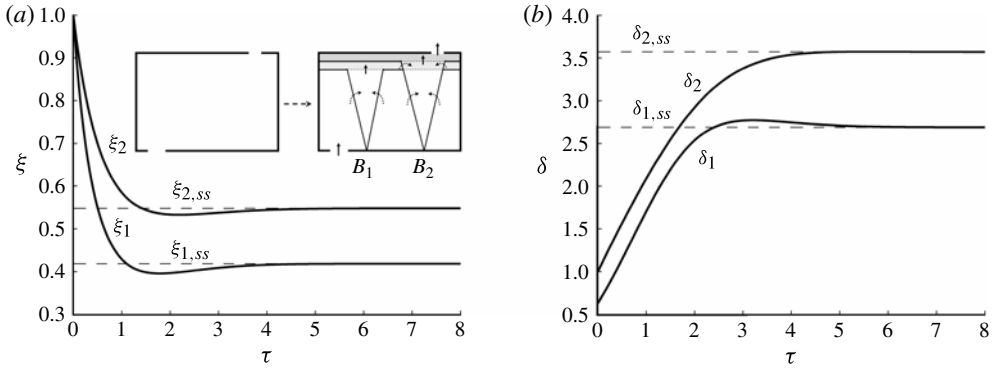


FIGURE 3. (*a*) Interface positions ξ_1, ξ_2 and (*b*) mean buoyancies δ_1, δ_2, for a filling flow when $A = 0.3$ and $\psi = 0.5$. The dashed lines are the steady solutions (1.3) and (1.4).

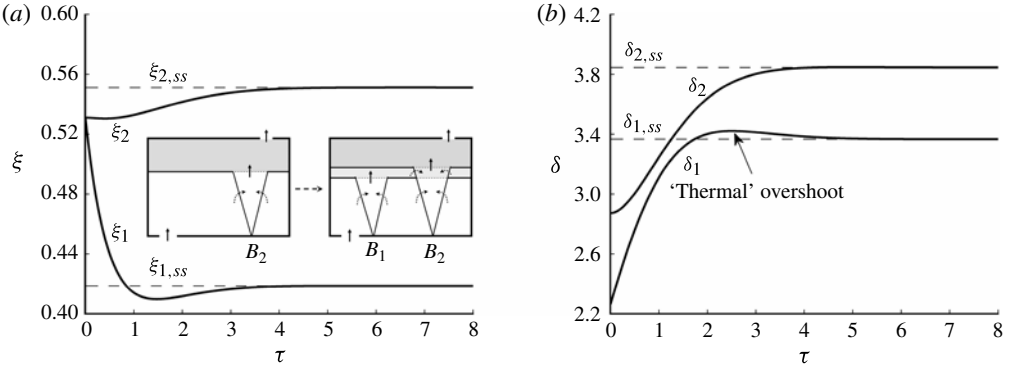


FIGURE 4. (*a*) Interface positions ξ_1, ξ_2 and (*b*) mean buoyancies δ_1, δ_2, for an ascending flow when $A = 0.3$ and $\psi = 0.7$. The dashed lines are the steady solutions (1.3) and (1.4).

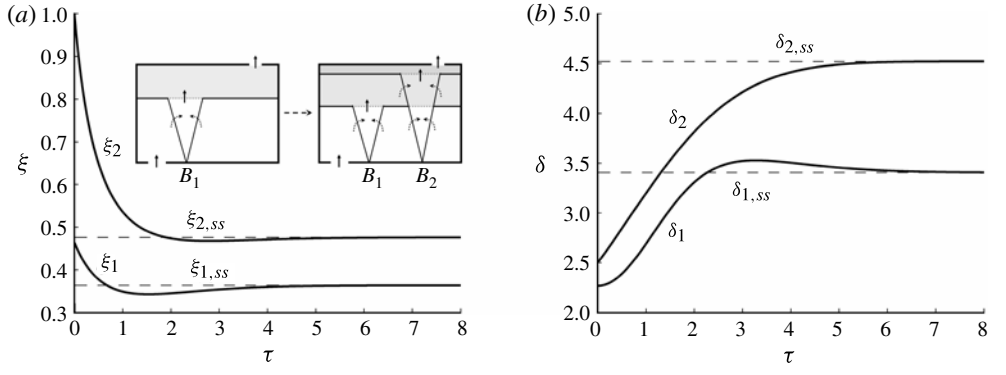


FIGURE 5. (*a*) Interface positions ξ_1, ξ_2 and (*b*) mean buoyancies δ_1, δ_2, for a descending flow when $A = 0.2$ and $\psi = 0.5$. The dashed lines are the steady solutions (1.3) and (1.4).

https://doi.org/10.1017/jfm.2013.579 Published online by Cambridge University Press

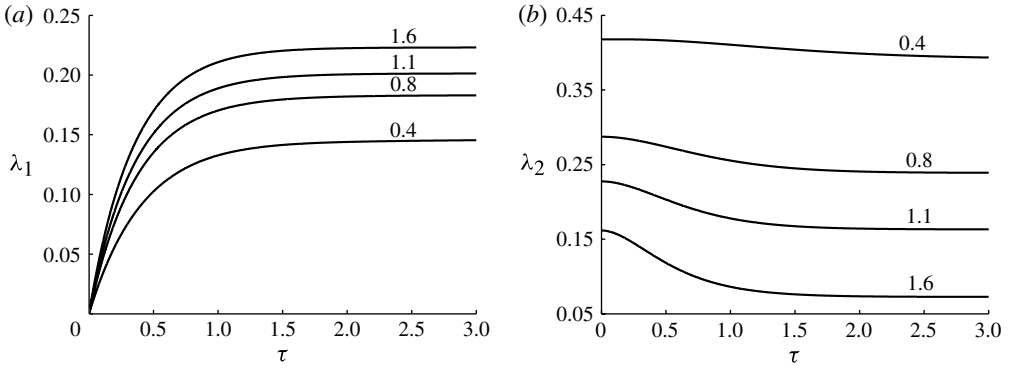


FIGURE 6. Layer depths for $A = \{0.4, 0.8, 1.1, 1.6\}$ and $\psi = 0.7$: (a) intermediate layer thickness, λ_1 ; (b) top layer thickness, λ_2.

descending flows also exhibit thermal overshoots, as illustrated in figures 3(b) and 5(b), respectively.

One of the key questions that this result raises is under what circumstances does the mean buoyancy of layer 1 overshoot its equilibrium value? In the following sections we establish that two conditions govern thermal overshoots and show that, for a given ψ, there exists a critical dimensionless area $A = A_{oh}$ ('oh' reading 'overheating') such that $\delta_1 > \delta_{1,ss}$ for $A < A_{oh}$. The results we present in the following figures are based on ascending flows and the values of $\{A, \psi\}$ are chosen so as to clearly illustrate the aspect of the flow under consideration. We later compare the dynamics of ascending and filling flows to determine the role of the initial conditions within the box on thermal overshoots. We also show that our theory on thermal overshoots applies to both ascending and filling flows. Finally, we establish the conditions necessary to induce a bulk overturning.

3.1. *Ascending flow pattern*

Figures 6(a) and 6(b) show the intermediate and top layer depths, $\lambda_1(\tau)$ and $\lambda_2(\tau)$, for four values of A. Evidently, when A is relatively large (e.g. $A = 1.6$), the stratification at large times is characterized by a thin top layer and a relatively deep intermediate layer. The initial interface positions ξ_{10} ($=\xi_{20}$) are located at higher elevations when A is relatively large and, specifically, layer 2 occupies only a small fraction of H. Consequently, on activation, the weaker plume rises to greater heights and, hence, supplies fluid of relatively low buoyancy at higher volume flow rates to layer 1 with increasing A. As a result, layer 1 initially deepens at a rapid rate. In contrast, layer 2 thins due to the increase in the net buoyancy Δ_N, (2.19), within the box and, hence, in the volume flux q_v purged from layer 2. Figure 6(a) shows that λ_1 increases to occupy approximately 25 % of the box height, whereas λ_2 reduces threefold to less than 7 % of the box height (figure 6b) and, hence, $\lambda_{1,ss} > \lambda_{2,ss}$. This highlights a practical result that may have appeared somewhat counter-intuitive at first sight, namely, that introducing a second heat source in a room with relatively large opening areas will potentially improve interior conditions; the original warm air layer thins significantly and a new deeper, but cooler, intermediate layer forms. Occupants exposed to the original warm layer would therefore experience lower temperatures despite the activation of an additional heat source.

https://doi.org/10.1017/jfm.2013.579 Published online by Cambridge University Press

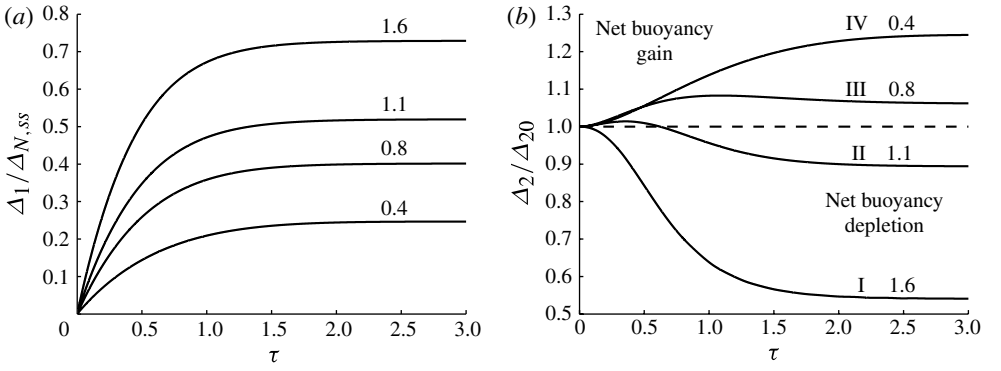


FIGURE 7. Net buoyancy ratios: (*a*) intermediate layer, $\Delta_1/\Delta_{N,ss}$, and (*b*) top layer, Δ_2/Δ_{20}, for $A = \{0.4, 0.8, 1.1, 1.6\}$ and $\psi = 0.7$. In (*b*), the region of net buoyancy gain/depletion in the top layer occurs above/below the dashed line.

When A is relatively small, the stratification at large times is characterized by a deep top layer and a relatively shallow intermediate layer (e.g. figure 6 for $A = 0.4$). As A decreases, layer 2 initially occupies a larger fraction of H. Consequently, the weaker plume rises a relatively short distance from the source before impingement on the interface. This results in the supply of buoyant fluid at low volume flow rates, yielding thin intermediate layers which deepen slowly. As before, layer 2 thins albeit at an ever decreasing rate as A decreases. In other words, initially deep top layers remain deep; note the near horizontal slope of the curves in figure 6(*b*) and that $\lambda_2 \approx \lambda_{20}$ as $A \to 0$. Moreover, when A is relatively small, the interfaces are closer to the sources and, hence, the buoyancies supplied to the layers are relatively large.

These results show that the development of the layer depths is strongly dependent on A which, as we shall see, also influences the way in which the net buoyancy within the box is apportioned between layers 1 and 2. To this end, figure 7(*a*) shows Δ_1 as a fraction of $\Delta_{N,ss}$. It is also informative to consider the time evolution of Δ_2 relative to its initial net buoyancy $\Delta_{20} = \Delta_2(\tau = 0)$ as plotted in figure 7(*b*). Depending on the value of A, Δ_2 can develop in four characteristically different ways: two in which the top layer is depleted of net buoyancy (scenarios I and II) and two in which there is a net buoyancy gain (scenarios III and IV). Scenario I classifies the response where $\Delta_2(\tau) < \Delta_{20}$ for $\tau > 0$. For example, when $A = 1.6$, layer 2 loses more than 40 % of its initial net buoyancy as the flow approaches steady state, thus giving rise to a weak contribution to the total driving force (figure 7*b*), whereas Δ_1 contributes more than 70 % of $\Delta_{N,ss}$ and, hence, layer 1 provides the dominant forcing. Scenario II occurs when Δ_2 increases for small τ, but subsequently decreases such that $\Delta_{2,ss} < \Delta_{20}$. Other values of A (e.g. $A = 0.8$) induce a scenario III response where Δ_2 increases to a maximum and decreases thereafter, but $\Delta_{2,ss} > \Delta_{20}$. Finally, scenario IV, which occurs when A is small, results in Δ_2 increasing monotonically so that $\Delta_2(\tau) > \Delta_{20}$. For example, when $A = 0.4$, layer 1 imposes a weak driving force, finally contributing only 20 % to $\Delta_{N,ss}$, whereas Δ_2 increases by approximately 25 % and layer 2 provides the dominant forcing.

The role of A in the development of these four scenarios is evident on considering the two end-members, namely, scenario I (attained for large A) and scenario IV (attained for small A). For scenario IV, the flow may be regarded as being 'choked' by the small top vent area; the box is predominantly 'filling' (cf. the limit of a true

https://doi.org/10.1017/jfm.2013.579 Published online by Cambridge University Press

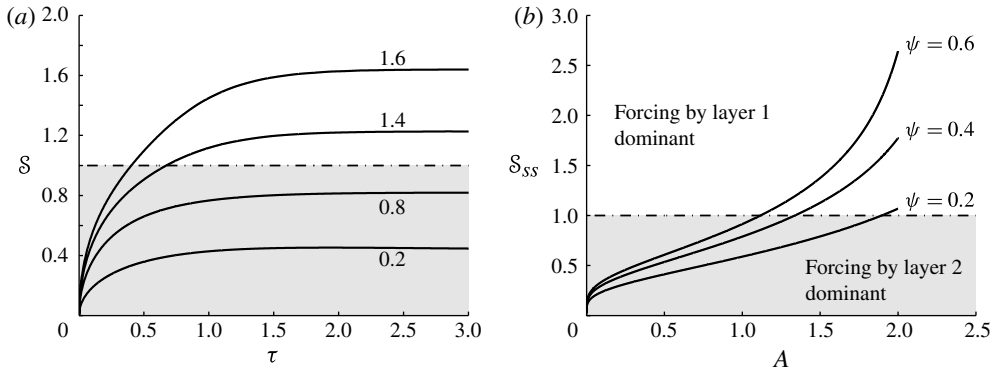


FIGURE 8. (*a*) Stratification parameter $\mathcal{S}(\tau)$ for $A = \{0.2, 0.8, 1.4, 1.6\}$ when $\psi = 0.7$. (*b*) $\mathcal{S}_{ss}$ as a function of A for $\psi = \{0.2, 0.4, 0.6\}$. Shaded areas show $\mathcal{S} < 1$, i.e. layer 2 providing the dominant forcing.

filling-box as $A \to 0$) and thus retains relatively large net buoyancy. For scenario I, there is greatly reduced choking and buoyant fluid is, by contrast, free to escape through the large vent at the top; the box is predominantly 'emptying' and thus retains relatively little net buoyancy. Consequently, increased choking increases Δ_N (for small A, the majority of the net buoyancy accumulates within layer 2 (figure 7)). Indeed, as A decreases, and thus the choking is enhanced, there is a strengthening interplay between the box-emptying and box-filling mechanisms, resulting in the more complex behaviours seen in scenarios II and III.

The flow behaviour can be elegantly captured via the stratification parameter $\mathcal{S} = \sqrt{\Delta_1/\Delta_2}$, which we recall, (2.20), is a measure of the relative contributions of layers 1 and 2 in driving the overall flow through the box. Figure 8(*a*) shows $\mathcal{S}(\tau)$ and figure 8(*b*) shows the stratification parameter at steady state, $\mathcal{S}_{ss}$, against A.

For $\mathcal{S}(\tau) \ll 1$ and $\mathcal{S}_{ss} \ll 1$ (shaded regions), layer 2 provides the dominant forcing and this occurs when A is relatively small. This is in accord with our previous result that for relatively small A, layer 2 gains net buoyancy ($\Delta_2 > \Delta_{20}$) and thereby imposes a strong driving force. Therefore, when $\mathcal{S} \ll 1$ an initially deep top layer remains deep and at steady state is of high net buoyancy ($\Delta_{N,ss} - \Delta_2 \ll 1$), whereas the intermediate layer formed is relatively shallow and of low net buoyancy ($\Delta_1/\Delta_{N,ss} \ll 1$); see figure 9(*a*).

For $\mathcal{S}(\tau) \gg 1$ and $\mathcal{S}_{ss} \gg 1$, layer 1 produces the dominant forcing and this occurs when A is relatively large, again consistent with the argument that for relatively large A, layer 2 loses net buoyancy ($\Delta_2 < \Delta_{20}$) and, thereby, imposes a weak driving force. Therefore, when $\mathcal{S} \gg 1$, an initially shallow top layer at $\tau = 0$ thins significantly as the flow approaches steady state. Furthermore, this top layer is of low net buoyancy ($\Delta_2/\Delta_{N,ss} \ll 1$), whereas the intermediate layer formed is relatively deep and of high net buoyancy ($\Delta_{N,ss} - \Delta_1 \ll 1$); see of figure 9(*b*).

Given that $\delta_{1,ss}/\delta_{2,ss}$ is an increasing function of ψ, (1.4), and $\mathcal{S}_{ss} \propto \sqrt{\delta_{1,ss}/\delta_{2,ss}}$, (2.20), the forcing provided by layer 1 increases with ψ as depicted in figure 8(*b*).

3.2. *Overshoot of the lower interface*

The lower interface overshoots its equilibrium position if the outflow (i.e. via the top opening) volume and buoyancy fluxes driven by the two buoyant layers do not

https://doi.org/10.1017/jfm.2013.579 Published online by Cambridge University Press

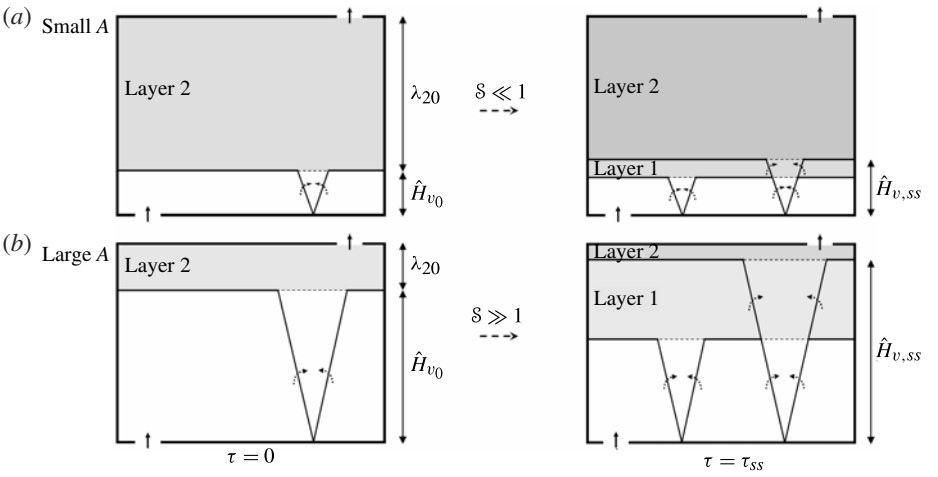


FIGURE 9. Schematics show the development of the stratification when (*a*) $\mathcal{S} \ll 1$ and (*b*) $\mathcal{S} \gg 1$. The left-hand column illustrates the initial state ($\tau = 0$) and the right-hand column the steady state ($\tau = \tau_{ss}$). The lengths $\hat{H}_{v_0}$ and $\hat{H}_{v,ss}$ are explained in § 3.3.1.

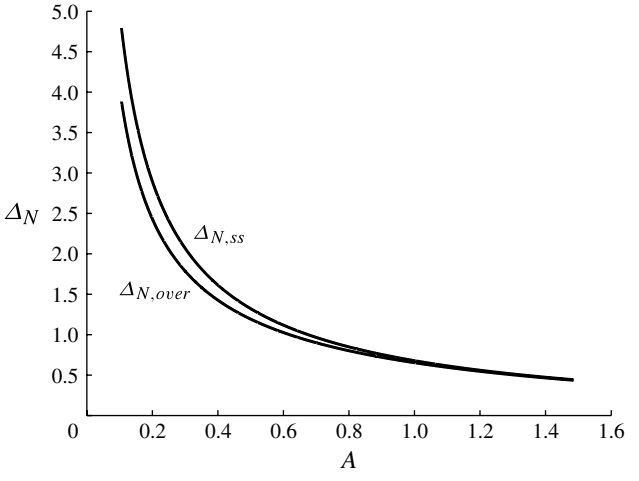


FIGURE 10. Net buoyancies $\Delta_{N,over}$ and $\Delta_{N,ss}$ as a function of A for $\psi = 0.5$.

equal the corresponding fluxes supplied to the layers by the two plumes at the instant $\tau = \tau_{over} < \tau_{ss}$ when ξ_1 first attains $\xi_{1,ss}$.

For the $\psi = 1$ problem, beginning with an initially uniformly cool box (i.e. $\delta(\hat{z}, \tau = 0) = 0$ for $0 \leqslant \hat{z} \leqslant 1$, where $\hat{z} = z/H$), Kaye & Hunt (2004) showed that this imbalance between box filling and box draining was due to insufficient layer buoyancy at the instant the ultimate steady interface level was first reached.

In the $\psi \neq 1$ problem, it is informative to determine the net buoyancy of the bulk buoyant layer, comprised of layers 1 and 2, at the instant $\tau = \tau_{over}$ (i.e. when overshoot first occurs), denoted as $\Delta_{N,over}$, and its value at steady state, $\Delta_{N,ss}$. Figure 10

https://doi.org/10.1017/jfm.2013.579 Published online by Cambridge University Press

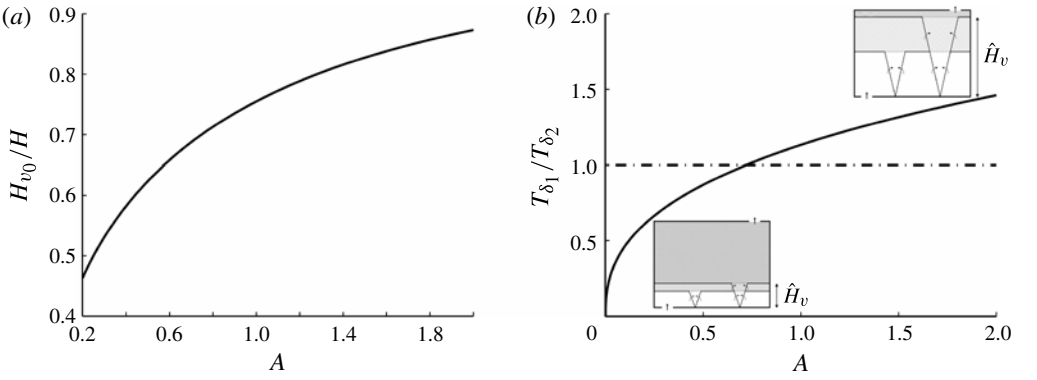


FIGURE 11. (*a*) Virtual box height $\hat{H}_{v_0} = H_v(t=0)/H$ as a function of A. (*b*) Ratio of buoyancy time scales $T_{\delta_1}/T_{\delta_2}$ as a function of A for $\psi = 0.6$.

shows $\Delta_{N,over}$ and $\Delta_{N,ss}$ as a function of A for $\psi = 0.5$. For relatively small A, $\Delta_{N,over} < \Delta_{N,ss}$, i.e. the bulk buoyant layer at $\tau = \tau_{over}$ has insufficient net buoyancy, relative to the steady-state value, in order to drive a displacement flow that equals the fluxes of volume and buoyancy supplied by the two plumes. Therefore, for $\tau > \tau_{over}$, the bulk buoyant layer continues to thicken resulting in $\xi_1 < \xi_{1,ss}$, i.e. overshooting its steady position. As A decreases, the difference $|\Delta_{N,ss} - \Delta_{N,over}|$ increases, giving rise to larger overshoots. As A increases, the difference diminishes, indicating that the box filling and box draining flows are closely balanced at $\tau = \tau_{over}$; for sufficiently large A, $\Delta_{N,over} = \Delta_{N,ss}$ and hence, no overshoot occurs.

3.3. *Thermal overshoots*

Thermal overshoots (3.1) are intrinsically linked to the time evolution of Δ_1 and Δ_2, occurring when δ_2 develops at a significantly slower rate than δ_1, such that a sufficient time lag is induced. Consequently, δ_1 first attains its steady value at an earlier time than δ_2 and subsequently exceeds, or overshoots, $\delta_{1,ss}$ before relaxing back to equilibrium.

We examine ascending flows to show that two conditions must be satisfied to induce the time lag and produce a thermal overshoot. In § 3.6 we show that the two conditions also apply if both plumes are activated simultaneously at $\tau = 0$ in an initially uniformly cool box (cf. 'filling' flows of figure 1). For the purposes of this discussion (§§ 3.3.1 and 3.3.2) we restrict our attention to 'small' opening areas and establish in § 3.5 the range of values of A that may be regarded as small.

3.3.1. *Thermal overshoot condition* 1

When A is small, the upper interface is low within the box, $h_2 \ll H$. Consequently, the rise of the weaker plume is restricted by the presence of this interface and, thus, may be regarded as being within the confines of a virtual box of reduced height $\hat{H}_v = H_v/H < 1$; a height which has a value $\hat{H}_{v_0} = \xi_{10}$ at $\tau = 0$ (see figure 9*a*). Figure 11(*a*) plots $\hat{H}_{v_0}$ as a function of A and, evidently, $\hat{H}_{v_0}$ rapidly decreases as A reduces. From plume theory, $G'_{11} \propto h_1^{-5/3}$ and $Q_{11} \propto h_1^{5/3}$ and, therefore, the weaker plume supplies fluid of relatively high buoyancy at low volume flow rates to fill an increasingly short virtual box as A decreases. Of course, $\hat{H}_v$ increases with τ as a consequence of ξ_2 ascending (figure 4*a*). However, as previously

https://doi.org/10.1017/jfm.2013.579 Published online by Cambridge University Press

established, $\lambda_2(\tau) \approx \lambda_{20}$ for relatively small A (figure 6*b*), thus $\hat{H}_v \approx \hat{H}_{v_0}$ for $\tau > 0$ and the upper interface effectively acts as a rigid boundary in terms of the development of layer 1; figures 11(*a*) and 6(*b*) show that $\hat{H}_v \approx 0.55$ when $A = 0.4$, restricting layer 1 to form within approximately half the box.

Confining the weaker plume within short virtual boxes results in the formation of shallow intermediate layers (figure 6*a*) of relatively low net buoyancy $\Delta_1/\Delta_{N,ss} \ll 1$ (figure 7*a*). Thus, $\mathcal{S} \ll 1$ and it becomes necessary for layer 2 to respond to the activation of the additional source. A response must occur, as the system, perturbed from a steady state at $\tau = 0$ by the input of an additional buoyancy flux B_1, needs to adjust so as to increase the buoyancy flux out of the top opening to equal the total $(B_1 + B_2)$ input in order to establish a new equilibrium. Layer 2 undergoes a significant increase in buoyancy (not in depth, see figure 6*b*). In other words, the top layer warms to increase the driving force it provides. As a result, Δ_2 evolves as per scenario III or IV, i.e. $\Delta_2(\tau)/\Delta_{20} > 1$ for $\tau > 0$ and there is a net buoyancy gain within layer 2 (figure 7*b*). We note that a scenario II response results in $\Delta_2/\Delta_{20} > 1$ only for small τ. Given that the time duration for which $\Delta_2/\Delta_{20} > 1$ is small compared with the time taken for the layer buoyancies to attain equilibrium, scenario II flows do not exhibit a thermal overshoot. Moreover, flows of this type, established only when A is sufficiently large such that $\mathcal{S}_{ss} \approx 1$, result in a depletion of the top layer's initial net buoyancy, i.e. $\Delta_{2,ss}/\Delta_{20} < 1$. Hence, the first condition that must be satisfied for there to be the possibility of a thermal overshoot stipulates

$$\phi(\tau) = \frac{\Delta_2(\tau)}{\Delta_{20}} = \frac{\lambda_2(\tau)\delta_2(\tau)}{\lambda_{20}\delta_{20}} > 1 \quad \text{for all } \tau > 0. \tag{3.2}$$

This is a necessary but not sufficient condition to produce an overshoot in δ_1. Note that figure 7(*b*) shows $\phi(\tau)$ and, evidently, (3.2) is satisfied only when A is sufficiently small. The first condition (3.2) has direct implications for the rates at which δ_1 and δ_2 develop, and leads us to the second condition.

3.3.2. *Thermal overshoot condition* 2

Given that the deep top layer thins (we recall that $\lambda_2(\tau) < \lambda_{20}$, figure 6*b*), its buoyancy δ_2 must increase in order for $\Delta_2 = \lambda_2\delta_2$ to increase and satisfy (3.2). For small A, $\lambda_2(\tau) \approx \lambda_{20}$ (figure 6*b*) and from (3.2), $\phi(\tau) \approx \delta_2(\tau)/\delta_{20}$ and $\phi_{ss} \approx \delta_{2,ss}/\delta_{20}$. Moreover, as A decreases, both $\phi(\tau)$ and ϕ_{ss} increase. Consequently, the increase in δ_2 required to re-establish equilibrium becomes larger; this is evident from figure 7(*b*) where we note that the vertical axis denotes $\phi \approx \delta_2/\delta_{20}$ when A is small. As a result, δ_2 evolves over a relatively long time scale prior to attaining its steady value $\delta_{2,ss}$. In contrast, δ_1 increases at a relatively rapid rate as layer 1 forms in close proximity to the weaker plume source (owing to a short virtual box) and, hence, takes a considerably shorter time to attain its steady value $\delta_{1,ss}$. This coupled effect gives rise to a time lag.

To provide further physical insight into the time lag, we consider the time scales that characterize the buoyancy development within layers 1 and 2, namely,

$$T_{\delta_1} = \sqrt{\frac{V_1^{1/3}}{G_1'|_{z=H_v}}} = \frac{S^{1/6}H_v}{B_1^{1/3}}, \quad T_{\delta_2} = \sqrt{\frac{V_2^{1/3}}{G_2'|_{z=H}}} = \frac{S^{1/6}H(1-\hat{H}_v)^{1/6}}{B_2^{1/3}}. \tag{3.3}$$

Here T_{δ_1} is the characteristic time for the (unventilated) virtual box of volume $V_1 = SH_v$ to fill with fluid of buoyancy equal to that in the weak plume at $z = H_v$, and T_{δ_2} the characteristic time for layer 2 of volume $V_2 = S(H - H_v)$ to fill with fluid

https://doi.org/10.1017/jfm.2013.579 Published online by Cambridge University Press

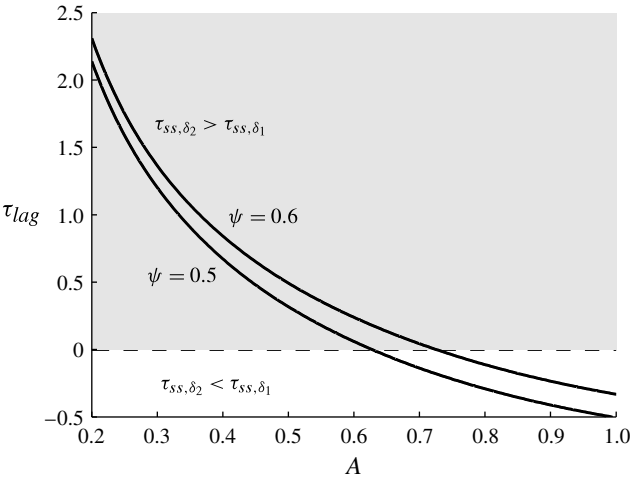


FIGURE 12. Time lag τ_{lag} as a function of A for $\psi = \{0.5, 0.6\}$. Shaded area shows $\tau_{lag} > 0$, i.e. when δ_2 lags behind δ_1.

of buoyancy equal to that in the strong plume at $z = H$. The ratio of the buoyancy time scales is

$$\frac{T_{\delta_1}}{T_{\delta_2}} = \frac{1}{\psi^{1/3}} \frac{\hat{H}_v}{(1-\hat{H}_v)^{1/6}}. \tag{3.4}$$

Figure 11(*b*) plots $T_{\delta_1}/T_{\delta_2}$ as a function of A for $\psi = 0.6$ taking $\hat{H}_v = \hat{H}_{v_0}$. Evidently, when A is small, $T_{\delta_1}/T_{\delta_2} \ll 1$ and hence the buoyancy of layer 1 evolves over a relatively short time scale compared with the buoyancy of layer 2.

To complement these scalings, the actual time taken for the layer buoyancies to first reach 99 % of their steady values $(\tau_{ss,\delta_1}, \tau_{ss,\delta_2})$ has been found from the numerical solutions to (2.22) and (2.23) and the time lag, defined as their difference, $\tau_{lag} = \tau_{ss,\delta_2} - \tau_{ss,\delta_1}$, determined. Plots of τ_{lag} as a function of A for $\psi = \{0.5, 0.6\}$ are shown in figure 12. As expected, the (shaded) region of the plot corresponding to $\tau_{lag} > 0$, where δ_2 takes a longer time than δ_1 to attain its steady value (i.e. $\tau_{ss,\delta_2} > \tau_{ss,\delta_1}$), is that for relatively small A. Evidently, as A decreases, the discrepancy between τ_{ss,δ_1} and τ_{ss,δ_2} increases further; we note in figure 12 that τ_{lag} can exceed two filling-box time scales (2.21). As a result, the top layer's buoyancy is less than its steady value $\delta_2/\delta_{2,ss} < 1$ at the time instant when the intermediate layer's buoyancy δ_1 first attains $\delta_{1,ss}$. Subsequently, δ_1 exceeds its steady value $(\delta_1/\delta_{1,ss} > 1)$ and attains a maximum before relaxing back to equilibrium. Upon examination of the initial (2.25) and steady (1.4) conditions, we note that

$$\frac{\delta_2/\delta_{2,ss}}{\delta_1/\delta_{1,ss}} = \begin{cases} \dfrac{1+\psi^{1/3}}{1+\psi} > 1 & \text{at } \tau = 0, \\ 1 & \text{at } \tau = \tau_{ss}, \end{cases} \tag{3.5}$$

i.e. the initial value of the buoyancy ratio (3.5) exceeds the steady value. Given that a positive time lag results in $\delta_2/\delta_{2,ss} < 1$ and $\delta_1/\delta_{1,ss} > 1$, it follows that for a thermal

https://doi.org/10.1017/jfm.2013.579 Published online by Cambridge University Press

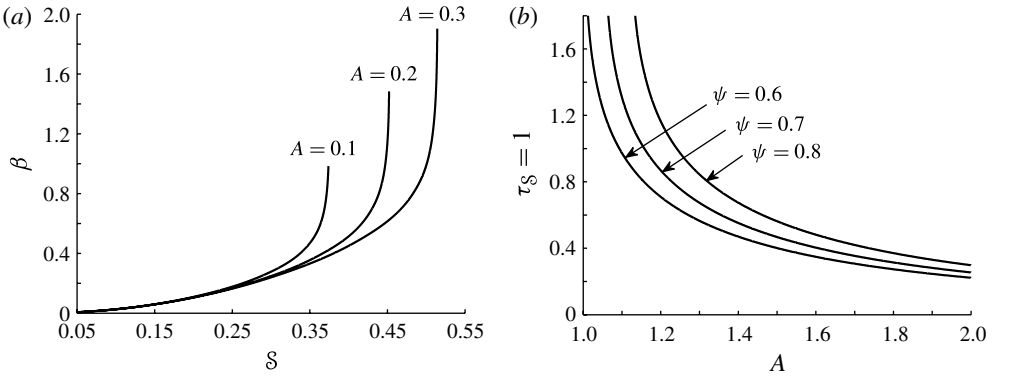


FIGURE 13. (*a*) Ratio of the rates of buoyancy development $\beta = (\mathrm{d}\delta_2/\mathrm{d}\tau)/(\mathrm{d}\delta_1/\mathrm{d}\tau)$ against $\mathcal{S}$ for $A = \{0.1, 0.2, 0.3\}$ and $\psi = 0.7$. (*b*) Time $\tau_{\mathcal{S}=1}$ at which $\mathcal{S} = 1$ as a function of A for $\psi = \{0.6, 0.7, 0.8\}$.

overshoot we require

$$\frac{\delta_2/\delta_{2,ss}}{\delta_1/\delta_{1,ss}} < 1. \tag{3.6}$$

Substituting for $\mathcal{S}$, (2.20), permits the second condition (3.6) to be written as

$$\frac{\mathcal{S}^2}{\left(\dfrac{\delta_{1,ss}}{\delta_{2,ss}}\dfrac{\lambda_1}{\lambda_2}\right)} > 1. \tag{3.7}$$

As we shall see in § 3.4, writing (3.6) in terms of $\mathcal{S}$ allows us to capture, in a single expression, the behaviour that gives rise to a thermal overshoot. Broadly speaking, our conditions for thermal overshoot stipulate that layer 2 must warm to increase its driving force (3.2) and continue to warm beyond the time layer 1 attains its equilibrium temperature (3.6).

3.4. *Dependence of time lag on the stratification*

When $\mathcal{S} \ll 1$ for $0 < \tau < \tau_{ss}$, layer 2 is relatively deep and layer 1 is shallow (see figure 9*a*), hence $\lambda_1/\lambda_2 \ll 1$. From (2.23*a*) and (2.23*b*), we note that

$$\frac{\mathrm{d}\delta_1}{\mathrm{d}\tau} \propto \frac{1}{\lambda_1}, \quad \frac{\mathrm{d}\delta_2}{\mathrm{d}\tau} \propto \frac{1}{\lambda_2}, \tag{3.8}$$

i.e. δ_2 develops at a relatively slow rate compared with δ_1. To illustrate this result, we plot $\beta = (\mathrm{d}\delta_2/\mathrm{d}\tau)/(\mathrm{d}\delta_1/\mathrm{d}\tau)$ against $\mathcal{S}$ in figure 13(*a*) for $0 < \tau < \tau_{oh}$, where $\tau = \tau_{oh}$ denotes the time instant at which δ_1 first exceeds $\delta_{1,ss}$. From (3.8), we note that $\beta \propto \lambda_1/\lambda_2$. Clearly, $\beta \ll 1$ when $\mathcal{S} \ll 1$ and therefore, owing to its rapid increase, the time taken for δ_1 to establish its equilibrium value is less than for δ_2. This gives rise to the time lag shown in figure 12. The dependence of the time lag on the stratification is also elegantly captured in (3.7). From (1.4), we note that $\delta_{1,ss}/\delta_{2,ss} = fn(\psi) < 1$. Therefore, for a given ψ, if $\mathcal{S} \ll 1$, we require $\lambda_1/\lambda_2 \ll 1$ (i.e. $\beta \ll 1$) in order to satisfy (3.7) and, hence, produce a time lag. In other words, δ_1 develops at a rapid rate and overshoots its steady value when layer 2 is dominant and layer 1 is relatively thin.

https://doi.org/10.1017/jfm.2013.579 Published online by Cambridge University Press

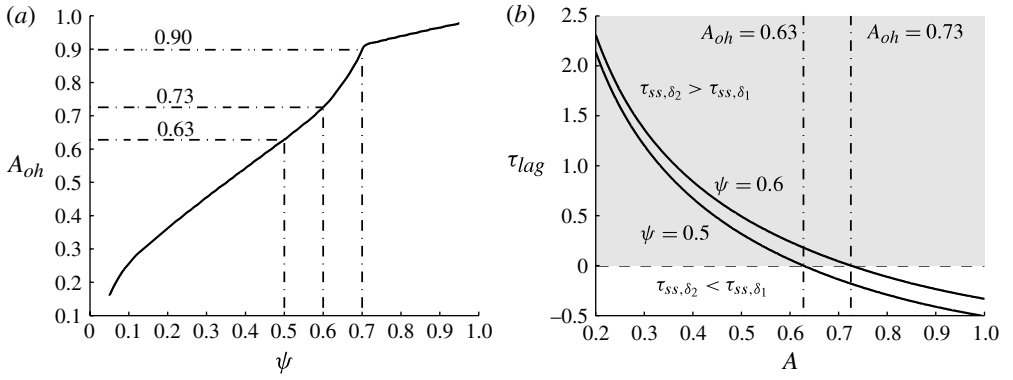


FIGURE 14. (*a*) Critical opening area A_{oh} for thermal overshoots as a function of ψ. Thermal overshoots occur for $A < A_{oh}$. Dot-dashed lines indicate A_{oh} for $\psi = \{0.5, 0.6, 0.7\}$. (*b*) Time lag τ_{lag} against A for $\psi = \{0.5, 0.6\}$. Dot-dashed lines indicate $A_{oh} = \{0.63, 0.73\}$ for $\psi = \{0.5, 0.6\}$ taken from (*a*).

When $\mathcal{S} \gg 1$, layer 1 is relatively deep (see figure 9*b*). However, during the early transients, irrespective of A, $\mathcal{S}(\tau) < 1$ and $\mathcal{S}(\tau) < \mathcal{S}_{ss}$ (figure 8*a*) as λ_1 and δ_1 are small relative to their respective steady values. Figure 13(*b*) plots the time $\tau_{\mathcal{S}=1}$ at which $\mathcal{S} = 1$ against A. Evidently, as A increases $\tau_{\mathcal{S}=1}$ rapidly decreases and hence, $\mathcal{S}$ exceeds unity at an earlier time. This is due to a rapid increase in λ_1 when A is relatively large (figure 6*a*). However, the buoyancy development of layer 1 lags behind the development of the layer's thickness as $\mathrm{d}\delta_1/\mathrm{d}\tau \propto 1/\lambda_1$. In contrast, λ_2 is small and a decreasing function of time and, hence, δ_2 increases at a relatively rapid rate given $\mathrm{d}\delta_2/\mathrm{d}\tau \propto 1/\lambda_2$. Consequently, when $\mathcal{S} \gg 1$, the time taken for δ_1 to attain $\delta_{1,ss}$ is greater than the time taken for δ_2 to attain $\delta_{2,ss}$. We note from figure 11(*b*) that when A is large, the ratio of the buoyancy time scales $T_{\delta_1}/T_{\delta_2} > 1$. This explains why $\tau_{lag} < 0$ for relatively large A (figure 12).

3.5. *Critical opening area for thermal overshoots*

It is of immediate interest to determine the region of $\{A, \psi\}$ space where thermal overshoots occur. For a given ψ, we decrease A (from $A = 2$) and determine the first value of $A = A_{oh}$ that satisfies the two thermal overshoot conditions, (3.2) and (3.7); this value is defined as the critical dimensionless area A_{oh}. Figure 14(*a*) plots $A_{oh}(\psi)$ for ascending flows; we also highlight the values of A_{oh} for $\psi = \{0.5, 0.6, 0.7\}$ as these are used in subsequent plots.

From our scaling arguments (3.4), we note that $T_{\delta_1}/T_{\delta_2}$ decreases as ψ increases, i.e. as the strength of the weak plume increases relative to the strong plume, layer 2 takes increasingly longer than layer 1 to attain its equilibrium buoyancy. This behaviour is also captured by (2.23*a*), which shows that $\mathrm{d}\delta_1/\mathrm{d}\tau$ increases with ψ, thus giving rise to a larger positive τ_{lag} (figure 12). Therefore, a larger value of A is required (i.e. taller virtual boxes are needed) to prevent a thermal overshoot as ψ increases. Hence, A_{oh} increases with ψ. In § 3.7 we provide arguments to explain the distinct change in the behaviour of A_{oh} when ψ is large (i.e. for $\psi \gtrsim 0.73$). We now present two sets of results that confirm the predictions of A_{oh} and, hence, show that the two conditions, (3.2) and (3.7), must be satisfied for δ_1 to exceed $\delta_{1,ss}$.

We deduced in §§ 3.3 and 3.4 that the time lag, τ_{lag}, governs thermal overshoots. Figure 14(*b*) shows τ_{lag} as a function of A for $\psi = \{0.5, 0.6\}$ and also plotted

https://doi.org/10.1017/jfm.2013.579 Published online by Cambridge University Press

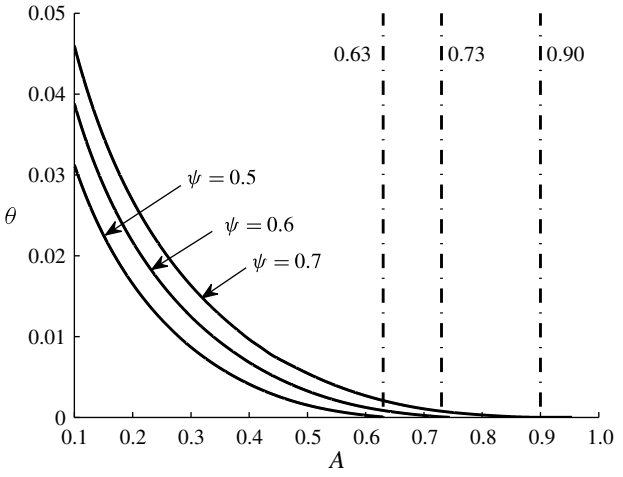


FIGURE 15. Degree of overheating θ versus A for $\psi = \{0.5, 0.6, 0.7\}$. The dot-dashed lines indicate $A_{oh} = \{0.63, 0.73, 0.90\}$ for $\psi = \{0.5, 0.6, 0.7\}$ taken from figure 14(*a*).

are the predicted values of A_{oh} corresponding to these two values of ψ taken from figure 14(*a*). For both values of ψ, it is evident that $\tau_{lag} \equiv 0$ when $A = A_{oh}$. Furthermore, for $A < A_{oh}$ we find that $\tau_{lag} > 0$. Therefore, when $A < A_{oh}$, the time taken for δ_2 to attain a value equal to $\delta_{2,ss}$ is greater than the time taken for δ_1 to attain $\delta_{1,ss}$, thus producing a time lag which gives rise to the thermal overshoot. Evidently, $\tau_{lag} < 0$ (i.e. $\tau_{ss,\delta_2} < \tau_{ss,\delta_1}$) for $A > A_{oh}$ and hence, δ_1 does not overshoot its steady value.

Denoting $\delta_{1,peak}$ as the maximum value of δ_1, we examine the 'degree of overheating', $(\delta_{1,peak} - \delta_{1,ss})$, expressed as a fraction of $\delta_{1,ss}$:

$$\theta = \frac{\delta_{1,peak} - \delta_{1,ss}}{\delta_{1,ss}}. \tag{3.9}$$

Figure 15 shows θ as a function of A for $\psi = \{0.5, 0.6, 0.7\}$. Also plotted are the predictions of A_{oh} corresponding to the three values of ψ taken from figure 14(*a*). For $A \geqslant A_{oh}$ it is evident that $\theta = 0$ and hence, $\delta_{1,peak} = \delta_{1,ss}$, (3.9), i.e. no thermal overshoot is produced. For $A < A_{oh}$, $\theta > 0$ and hence, $\delta_{1,peak} > \delta_{1,ss}$, i.e. a thermal overshoot is produced. As A decreases, τ_{lag} increases dramatically (figure 12) and, as a result, θ increases (figure 15).

We have shown that the values of A_{oh} satisfying the two theoretical conditions, (3.2) and (3.7), are identical to those that give $\tau_{lag} = 0$ and $\theta = 0$, thus illustrating the agreement between our thermal overshoot theory (§ 3.3) and the numerical results.

3.6. *Comparison of ascending and filling flows*

Our examination of the thermal overshoot raises the question of what effect do the initial conditions have on $\delta_{1,peak}$? We now compare the dynamics of ascending and filling flows to address this question and show that our theory on thermal overshoots (§ 3.3) applies to both flows.

Figure 16(*a*) shows the degree of overheating (3.9) for ascending and filling flows, θ_a and θ_f, respectively, as a function of A. From Linden & Cooper's (1996) steady solution, (1.3) and (1.4), we recall that $\delta_{1,ss}$ and $\delta_{2,ss}$ are dependent only on A and ψ. However, for a given $\{A, \psi\}$ it is evident that $\theta_f > \theta_a$ and, hence, $\delta_{1,peak}$ is greater

https://doi.org/10.1017/jfm.2013.579 Published online by Cambridge University Press

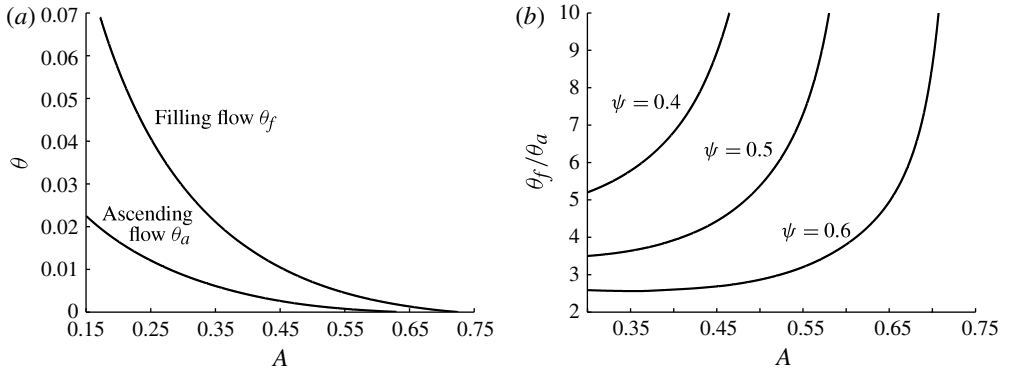


FIGURE 16. (*a*) Degree of overheating for ascending and filling flows, θ_a and θ_f, for $\psi = 0.5$ and (*b*) θ_f/θ_a for $\psi = \{0.4, 0.5, 0.6\}$ versus A.

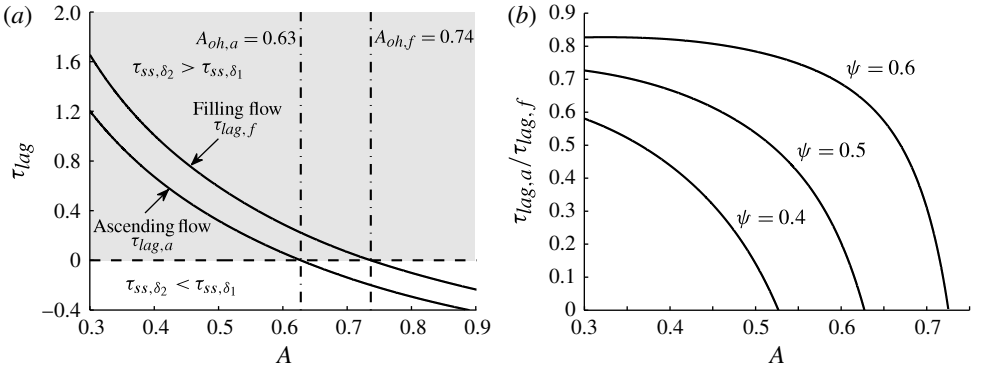


FIGURE 17. (*a*) Time lag for ascending and filling flows, $\tau_{lag,a}$ and $\tau_{lag,f}$, for $\psi = 0.5$, and (*b*) $\tau_{lag,a}/\tau_{lag,f}$ for $\psi = \{0.4, 0.5, 0.6\}$ versus A. Shaded area in (*a*) shows $\tau_{lag} > 0$.

when both plumes are activated simultaneously. This suggests that thermal overshoots are dependent on the time history of the flow. To reinforce this result, the variation of θ_f/θ_a with A is shown in figure 16(*b*) and we note that $\theta_f/\theta_a > 1$ for all values of $\{A, \psi\}$ considered. Evidently, the initial conditions have a dramatic effect on $\delta_{1,peak}$. For example, when $\psi = 0.5$ and $A = 0.3$, $\theta_f/\theta_a \approx 3.5$ (figure 16*b*), i.e. the degree of overheating is approximately three-and-a-half times greater for a 'filling' flow than for an 'ascending' flow.

To explain why $\theta_f > \theta_a$ we compare the relative magnitudes of τ_{lag} for ascending and filling flows. Figure 17(*a*) plots $\tau_{lag,a}$ and $\tau_{lag,f}$ as a function of A for $\psi = 0.5$. Also plotted are the predicted values of the critical areas, $A_{oh,a}$ and $A_{oh,f}$, calculated using (3.2) and (3.7) (see § 3.5). Thermal overshoots occur in the shaded region of the plot where $\tau_{lag} > 0$, i.e. when δ_2 lags behind δ_1. Moreover, in this region it is evident that the time lag is greater for filling flows ($\tau_{lag,f} > \tau_{lag,a}$). Restricting our attention to $A < A_{oh,a}$, figure 17(*b*) plots the variation of $\tau_{lag,a}/\tau_{lag,f}$ with A. Clearly, $\tau_{lag,a}/\tau_{lag,f} < 1$ and, hence, the rate of development of δ_2 is slower for filling flows. As a result, the time taken for $\delta_{2,f}$ to attain equilibrium exceeds the time taken for $\delta_{2,a}$ to attain the same steady state. In contrast, the rate of development of δ_1 is faster for filling flows

https://doi.org/10.1017/jfm.2013.579 Published online by Cambridge University Press

and, hence, the time taken for $\delta_{1,f}$ to attain equilibrium is less than the time taken for $\delta_{1,a}$ to attain the same steady state. Given that θ increases with τ_{lag} (figures 12 and 15) and $\tau_{lag,f} > \tau_{lag,a}$ (figure 17*b*), $\theta_f > \theta_a$.

In developing our thermal overshoot theory (§ 3.3), we restricted our attention to ascending flows. However, we now show that our theory also applies to filling flows by considering the case where the two unequal plumes (with $\psi = 0.5$) are activated simultaneously at $\tau = 0$ in an initially unstratified box. For this filling flow, we used the two thermal overshoot conditions, (3.2) and (3.7), to determine the dimensionless area $A_{oh,f} = 0.74$. Examining figure 17(*a*), which shows $\tau_{lag,f}$ as a function of A for $\psi = 0.5$, we find that $\tau_{lag,f} \equiv 0$ when $A = A_{oh,f} = 0.74$ and moreover, $\tau_{lag,f} > 0$ when $A < 0.74$. Furthermore, as a result of this time lag, we find (figure 16*a*) that $\theta_f > 0$ only for $A < 0.74$ and $\theta_f = 0$ for $A \geqslant 0.74$. In other words, filling flows exhibit a thermal overshoot for $A < A_{oh,f}(\psi)$.

From a physical perspective, the result $\theta_f > \theta_a$ is consistent with our thermal overshoot theory. For filling flows the plumes supply an initially unstratified box of zero net buoyancy $\Delta_N(\tau = 0) = 0$ whereas, for ascending flows, $\Delta_N(\tau = 0) = \Delta_{20} > 0$. Therefore, when A is small, the increase required in Δ_2 is significantly larger for filling flows. Consequently, the time scale over which Δ_2 and δ_2 evolve is considerably longer. This results in $\tau_{lag,a}/\tau_{lag,f} < 1$, which gives rise to $\theta_f/\theta_a > 1$.

3.7. *Overturning*

In § 3.5 we showed that thermal overshoots occur for $A < A_{oh}$ as a result of a lag between the time evolution of the two layer buoyancies. The time lag increases dramatically as A decreases and for sufficiently small A we predict that δ_1 increases at such a rapid rate during the early transients that

$$\delta_1 = \delta_2 \quad \text{at } \tau = \tau_{ot}, \tag{3.10}$$

where τ_{ot} denotes the time at which 'overturning' first occurs. We note that (3.10) prescribes the condition for overturning for filling, ascending and descending flows. For $\tau > \tau_{ot}$, the system would be statically unstable and a bulk overturning of the buoyant layers induced. Consequently, our model (§ 2), based on a stable three-layer stratification, is only valid for $\tau < \tau_{ot}$. A new set of 'initial' conditions would need to be prescribed to describe the subsequent transients, the dynamics of which are complex and beyond the immediate scope of this paper. Practically, if overturning does occur, at that instant no single plume dominates the layering. Thereafter, despite a breakdown in stratification, two interfaces are likely to be re-established as the plumes are of unequal strengths.

Similar to the thermal overshoot experienced by layer 1, overturning is intrinsically related to the rates at which δ_1 and δ_2 develop. In order for (3.10) to be satisfied, we require $\mathrm{d}\delta_1/\mathrm{d}\tau \gg \mathrm{d}\delta_2/\mathrm{d}\tau$ for $\tau < \tau_{ot}$. For a given ψ we established, using a numerical search, the maximum value of A for which (3.10) occurs and we define this to be the critical area A_{ot} that induces overturning, so that $\delta_1 = \delta_2$ at $\tau = \tau_{ot}$ when $A < A_{ot}$. Figure 18 shows A_{oh} and A_{ot} as functions of ψ and identifies the regions of $\{A, \psi\}$ space where localized overheating and bulk overturning motions are induced for ascending flows. Evidently, as ψ increases, the dominant flow feature transitions from localized overheating to bulk overturning. For example, when $A = 0.2$ and $\psi = 0.4$, overheating is induced, whereas for the same A, increasing the source strength ratio to $\psi = 0.8$ gives rise to overturning. Therefore, when $A < A_{ot} < A_{oh}$, the increase in δ_1 is so rapid that δ_1 exceeds δ_2 before overshooting its steady value $\delta_{1,ss}$, i.e. overturning occurs prior to overheating.

https://doi.org/10.1017/jfm.2013.579 Published online by Cambridge University Press

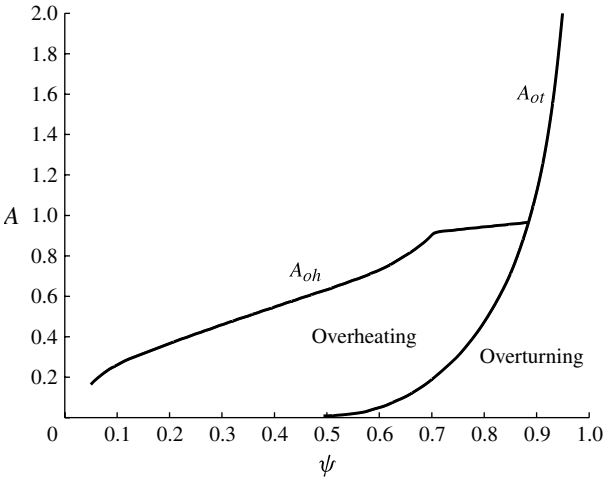


FIGURE 18. Ascending flow. Critical opening areas for overheating and overturning, $A_{oh}(\psi)$ and $A_{ot}(\psi)$.

The distinct change in the behaviour of A_{oh} when ψ is large may now be explained by identifying the dominant parameter controlling the time evolution of δ_1 in the limits of small ψ (i.e. $\psi \ll 1$) and large ψ (i.e. $\psi \sim 1$). For small ψ, the rapid accumulation of buoyancy within layer 1, in the context of thermal overshoots, is controlled primarily by A; we note that when ψ is small, A_{oh} is small and, hence, thermal overshoots are induced by confining the weaker plume to a short virtual box (§ 3.3.1). For large ψ, the rapid increase in δ_1 is controlled predominantly by ψ itself as the weaker plume, now comparable in strength to the stronger plume, supplies fluid of relatively high buoyancy to layer 1 (§ 3.5). In this limit, relatively small increments in ψ (for a given $A < A_{oh}$) can result in bulk overturning being induced as opposed to localized overheating. Therefore, as $\psi \to 1$, the parameter controlling the rate of increase of δ_1, and hence overheating and overturning, changes from A to ψ. As a result, the behaviour of A_{oh} is characteristically different when ψ is large. For sources of equal strength ($\psi = 1$), a two-layer stratification is established, i.e. $\delta_{10} = \delta_{20}$, (2.25). Therefore, as $\psi \to 1$, $\tau_{ot} \to 0$ and hence, $A_{ot} \to \infty$ (figure 18).

In summary, overheating occurs for $A_{ot} < A < A_{oh}$ and overturning for $A < A_{ot}$. Based on curves of best fit to our model predictions in figure 18,

$$A_{oh} \approx \begin{cases} \psi + 0.15 & \text{for } 0.1 < \psi \lesssim 0.7, \\ 0.25\psi + 0.75 & \text{for } 0.7 < \psi \lesssim 0.88, \end{cases} \quad A_{ot} \approx \frac{9}{4}\frac{(\psi - 0.5)^2}{(1-\psi)^{1/2}} \quad \text{for } \psi \geqslant 0.5. \tag{3.11}$$

Interestingly, (3.11) reveals that flows exhibit overheating or overturning irrespective of the cross-sectional area S of the box. However, the times at which these flow features occur depend on S.

4. Conclusions

We examined theoretically the transient buoyancy-driven displacement flow in a ventilated box that is initiated and maintained by two localized sources of unequal strength (B_1 and $B_2 > B_1$) which produce turbulent (non-interacting) plumes. Our

https://doi.org/10.1017/jfm.2013.579 Published online by Cambridge University Press

model describes the time evolution of the resulting three-layer stratification and shows that the dimensionless mean buoyancy of the intermediate (i.e. middle) layer, δ_1, can exceed its steady value, $\delta_{1,ss}$, for a significant duration of the transients giving rise to a thermal overshoot, in other words a region of 'localized overheating'. Coupled with this surplus buoyancy is an excess in the total depth of the buoyant fluid region which results from the descent of the lower interface below its equilibrium position. Interestingly, the stratification may break down owing to a bulk overturning of the two buoyant layers, induced if the mean buoyancy of the intermediate layer δ_1 exceeds that of the top layer, δ_2.

The dynamics of these flows depend on the dimensionless opening area A and the source strength ratio $\psi = B_1/B_2 < 1$, and their development is sensitive to the initial stratification within the box. We have shown that the general flow behaviour can be characterized by the stratification parameter $\mathcal{S}$, a measure of the relative buoyancy-induced velocities of the intermediate and top layers. For $\mathcal{S} \ll 1$ a relatively deep top layer dominates the fluid motion, whereas for $\mathcal{S} \gg 1$ a relatively deep intermediate layer produces the dominant forcing. Moreover, we have identified that thermal overshoots and bulk overturning occur in the limit of small $\mathcal{S}$, and thus one can broadly classify the complex dynamics based on a single parameter.

We have developed a theory for thermal overshoots centred around the time lag between the development of the two layer buoyancies. We have shown that when A is small, and as a consequence the top layer provides the dominant forcing ($\mathcal{S} \ll 1$), the layer buoyancies evolve on two characteristically different time scales; the time taken for the top layer to warm and for its buoyancy to attain equilibrium is large compared with the intermediate layer, thus giving rise to the time lag. We deduced that two conditions control this behaviour and are necessary to produce the lag. Applying our theory to ascending flows, which occur when a steady two-layer stratification is first established by a single plume and a second weaker plume is then activated, we determined the maximum dimensionless opening area, $A_{oh}(\psi)$, for which localized overheating occurs. Theoretical predictions of A_{oh} show good agreement with numerical results from our model and indicate that a thermal overshoot will occur for $A < A_{oh}$.

Whilst we have primarily examined interface overshoots, thermal overshoots and overturning in the context of ascending flows, these three features are also predicted when both plumes are simultaneously activated in a uniformly cool box ('filling flows'), and when the stronger plume is activated subsequent to the weaker plume establishing a steady two-layer stratification ('descending flows'). Indeed, in principle one could examine any number of initial states following the approach we have developed; such an analysis may shed further light on the sensitivity of these features to the initial conditions within the box.

The mathematical model developed may be used to: (*a*) estimate the time-dependent temperature profiles in ventilated rooms heated simultaneously by sources of unequal strength; and (*b*) predict the transient evolution of the ventilation flow from one (potential) steady regime to another resulting from the activation of a weaker or stronger heat source. Of practical significance in the design of ventilation strategies is our result that air temperatures within the intermediate layer may, for a significant duration, exceed (or overshoot) those in the steady state. The need for designers to consider these time-dependent flows, rather than solely the steady states, is thereby crucial to avoid regions which locally overheat and, thereby, cause discomfort for occupants.

https://doi.org/10.1017/jfm.2013.579 Published online by Cambridge University Press

Whilst thermal overshoots are strongly dependent on the sequence in which the two plumes are activated, several other factors may influence the evolution of the stratification. If the weaker plume source is elevated, the intermediate layer will receive a supply of highly buoyant fluid owing to its formation closer to the source, and hence one may anticipate more pronounced thermal overshoots. Strong external winds that oppose the buoyancy-driven flow will cause a rapid accumulation of buoyancy within the box, thus possibly extending the region of $\{A, \psi\}$ space where thermal overshoots and overturning are realized. Flows initiated and maintained by $n(>2)$ sources of different strengths that give rise to n buoyant layers may exhibit thermal overshoots in multiple layers. Moreover, 'localized overturning' may be induced if the buoyancy of a layer exceeds that of the layer above whilst all other regions remain stably stratified. These extensions to our work offer challenging avenues for future research.

Appendix. Improved theoretical model

We now extend the model (§ 2) to account for the stronger plume behaviour within layer 1 and the turbulent entrainment flux Q_e due to fountain–interface interaction.

A.1. *Analysis of the distributed stronger plume within layer* 1

At $z = h_1$, the stronger plume (of source buoyancy flux B_2) experiences a reduction in buoyancy flux due to the density change in the environment. To predict Q_{22}, we analyse the stronger plume in two stages: (i) as a pure plume within layer 0 with source conditions $(Q_2(z=0)=0,\ M_2(z=0)=0, B_2(z=0)=B_2)$; and (ii) as a distributed plume within layer 1 with source conditions (Q_{21}, M_{21}, B_2') at $z = h_1$. Here, M denotes momentum flux and $B_2'(t) = B_2 - g_1'(t)Q_{21}(t)$ the time-varying source buoyancy flux of the distributed plume.

Scase *et al.* (2006) showed that, except for regions close to the source, the behaviour of a turbulent plume is largely unaffected by a sudden decrease in the source strength. Therefore, for simplicity we assume the stronger plume is quasi-steady at each time instant. The equations for the conservation of volume flux Q_2, momentum flux M_2 and buoyancy flux B_2' of the distributed plume are based on the steady plume theory of Morton *et al.* (1956) and, for top-hat profiles, take the form

$$\frac{\mathrm{d}Q_2}{\mathrm{d}z'} = 2\alpha\pi^{1/2}M_2^{1/2}, \quad \frac{\mathrm{d}M_2}{\mathrm{d}z'} = \frac{B_2'Q_2}{M_2}, \quad \frac{\mathrm{d}B_2'}{\mathrm{d}z'} = 0, \tag{A 1}$$

where z' is the vertical coordinate with origin at the level $z = h_1$ of the lower interface. We scale Q_2 and M_2 on the fluxes of volume and momentum at $z = H$ within a pure plume rising from a source at $z = 0$ of buoyancy flux B_2 through a uniform ambient environment $g_0' = 0$, denoted by $Q_{2,H}$ and $M_{2,H}$, respectively. From the similarity solutions of Morton *et al.* (1956), we can write

$$Q_{2,H} = \pi\left(\frac{6\alpha}{5}\right)^{4/3}\left(\frac{3}{4\pi}\right)^{1/3}B_2^{1/3}H^{5/3}, \quad M_{2,H} = \pi\left(\frac{6\alpha}{5}\right)^{2/3}\left(\frac{3}{4\pi}\right)^{2/3}B_2^{2/3}H^{4/3}. \tag{A 2}$$

We scale B_2' on B_2, z' on H and introduce the non-dimensional buoyancy flux of the distributed plume f_2' and vertical coordinate $\hat{z}'$, accordingly

$$f_2' = \frac{B_2'}{B_2} = 1 - \delta_1\xi_1^{5/3}, \quad \hat{z}' = \frac{z'}{H}. \tag{A 3}$$

https://doi.org/10.1017/jfm.2013.579 Published online by Cambridge University Press

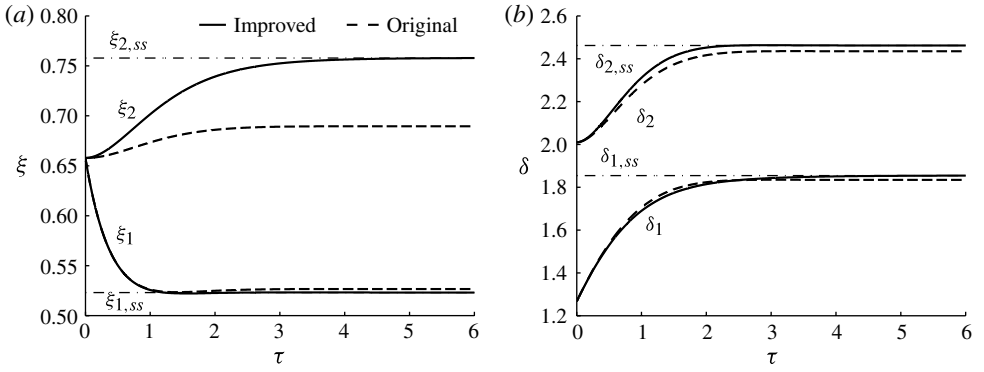


FIGURE 19. (*a*) Interface positions ξ_1, ξ_2 and (*b*) mean buoyancies δ_1, δ_2 for $A = 0.6$ and $\psi = 0.5$, for the improved and original models for an ascending flow. The dot-dashed lines show the steady-state predictions of Cooper & Linden (1996).

Non-dimensionalizing (A 1) gives

$$\frac{\mathrm{d}q_2}{\mathrm{d}\hat{z}'} = \frac{5}{3} m_2^{1/2}, \quad \frac{\mathrm{d}m_2}{\mathrm{d}\hat{z}'} = \frac{4}{3}\frac{f_2' q_2}{m_2}, \quad \frac{\mathrm{d}f_2'}{\mathrm{d}\hat{z}'} = 0, \tag{A 4}$$

where $q_2 = Q_2/Q_{2,H}$ and $m_2 = M_2/M_{2,H}$. To determine $q_2(\hat{z}' = \lambda_1) = q_{22}$ at each time instant, we solve (A 4) with source conditions $(q_2(z' = 0) = \xi_1^{5/3}, m_2(z' = 0) = \xi_1^{4/3}, f_2'(z' = 0) = f_2')$.

A.1.1. *Analysis of the results*

Numerical solutions of the governing equations (2.22*a*,*b*) and (2.23*a*,*b*), where q_{22} is now obtained by solving (A 4) at each time step, have been obtained for the three sets of initial conditions (§ 2.1) using a fourth-order Runge–Kutta finite-difference scheme. In the following discussion, we refer to our model in § 2 as the 'original' model and our model in § A.1, which accounts for the stronger plume behaviour within layer 1, as the 'improved' model.

Figures 19(*a*) and 19(*b*), respectively, show the two interface positions and mean layer buoyancies as functions of τ for an ascending flow when $A = 0.6$ and $\psi = 0.5$ for the original and improved models. Also plotted are the steady predictions of Cooper & Linden (1996) who account for the reduction in B_2 using a virtual origin correction. Comparing the two model predictions (figure 19), it is evident that ξ_1, δ_1 and δ_2 are little affected by the reduction in B_2. Moreover, for a significant duration of the transients (approximately one filling-box time scale), the predictions of the original and improved models for ξ_1 and δ_1 are graphically indistinguishable. Therefore, our theory on thermal overshoots (§ 3.3) is not influenced by the reduction in B_2. The original model does however markedly underestimate ξ_2. For $0 < \psi < 0.3$, differences in the predictions of ξ_2 are relatively small (less than 5 %). However, as ψ increases, the differences become larger and increase to a maximum of 20 % as $\psi \to 1$. The reason for the underprediction is discussed by Linden & Cooper (1996).

We have used the improved model to obtain the variation of θ with A and this is plotted in figure 20 for four values of ψ. Comparing these predictions of θ with those of the original model (figure 15), we note that there is a quantitative change in the values of A for which thermal overshoots occur. However, the magnitudes of θ $(0 < \theta < 0.05)$ predicted by the two models are comparable. Moreover, the basic qualitative variation of θ with A is unchanged when we account for the reduction

https://doi.org/10.1017/jfm.2013.579 Published online by Cambridge University Press

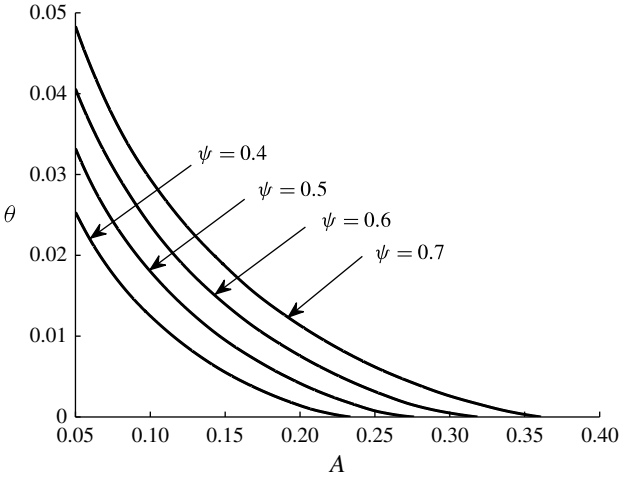


FIGURE 20. Predictions of θ for $\psi = \{0.4, 0.5, 0.6, 0.7\}$ obtained from our improved model.

in B_2. Hence, the dynamics that govern thermal overshoots (§ 3.3) is the same for both models.

A.2. *Turbulent entrainment due to fountain-interface interaction*

Fluid from the weaker plume rises within layer 1 as a dense fountain, driven by its 'source' momentum flux at $\hat{z} = \xi_1$, and provided its rise height exceeds λ_1, it impinges on the upper interface. The impingement (and any subsequent penetration into layer 2) gives rise to a vertical downward transport of buoyant fluid at a rate $g_2' Q_e$ across the upper interface into layer 1.

Baines (1975), who considered a turbulent plume incident on an interface separating two initially homogeneous layers of different density, deduced from experimental measurements that the dimensionless entrainment flux $E = Q_e/Q_{12}$ is proportional to the cube of the interfacial Froude number $Fr_i = w_i/(\sqrt{r_i \Delta g'})$. Here, w_i and r_i denote the vertical velocity and radius, respectively, of the plume (or fountain) at the interface and $\Delta g' = g_2' - g_1'$. Kumagai (1984) considered the same experimental set up as Baines (1975) and proposed an empirical relationship of the form

$$E = \frac{Fr_i^3}{1 + 3.1 Fr_i^2 + 1.8 Fr_i^3}. \tag{A 5}$$

From (A 5) we note that $E \propto Fr_i^3$ for $Fr_i \ll 1$ and $E \to 0.56$ when $Fr_i \gg 1$. Lin & Linden (2005) examined the impingement of a jet on a steady interface and found that E is approximately constant at $E \approx 0.65$ for $1 \lesssim Fr_i \lesssim 2.2$. We adopt the empirical model of Kumagai (1984), (A 5), to quantify E. In the problem under consideration, we find that Q_e is relatively small compared with the other volume fluxes of interest. Hence, the choice of the entrainment model is relatively unimportant.

Applying conservation of volume and buoyancy for each layer:

$$\frac{\mathrm{d}h_1}{\mathrm{d}t} = \frac{Q_v - Q_{11} - Q_{21}}{S}, \quad \frac{\mathrm{d}h_2}{\mathrm{d}t} = \frac{Q_v + Q_e - Q_{22}}{S}, \tag{A 6}$$

$$\frac{\mathrm{d}g_1'}{\mathrm{d}t} = \frac{Q_{11}(G_{11}' - g_1') + Q_e(g_2' - g_1')}{S(h_2 - h_1)}, \quad \frac{\mathrm{d}g_2'}{\mathrm{d}t} = \frac{B_2 + g_1'(Q_{22} - Q_{21}) - g_2' Q_{22}}{S(H - h_2)}. \tag{A 7}$$

https://doi.org/10.1017/jfm.2013.579 Published online by Cambridge University Press

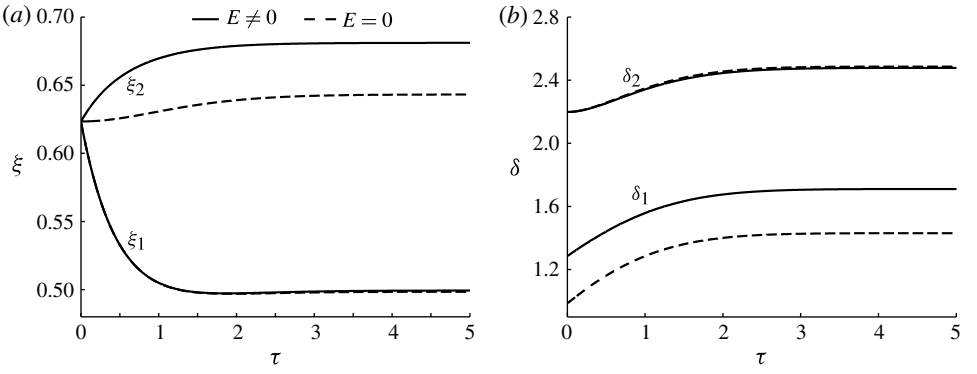


FIGURE 21. (*a*) Interface positions ξ_1, ξ_2 and (*b*) mean buoyancies δ_1, δ_2 as functions of τ with $E \neq 0$ and $E = 0$ for $A = 0.5$ and $\psi = 0.3$.

Non-dimensionalizing (A 6) and (A 7), we find that the time rates of change of ξ_1 and δ_2 are independent of E and, hence, $\mathrm{d}\xi_1/\mathrm{d}\tau$ and $\mathrm{d}\delta_2/\mathrm{d}\tau$ are governed by (2.22*a*) and (2.23*b*). From (A 6) and (A 7), the equations governing the evolution of ξ_2 and δ_1 are

$$\frac{\mathrm{d}\xi_2}{\mathrm{d}\tau} = A\Delta_N^{1/2} - q_{22} + Eq_{12}, \quad \frac{\mathrm{d}\delta_1}{\mathrm{d}\tau} = \frac{\psi - \psi^{1/3}\delta_1\xi_1^{5/3} + Eq_{12}(\delta_2 - \delta_1)}{\lambda_1}, \quad \text{(A 8}a,b\text{)}$$

where $q_{12} = Q_{12}/Q_{2,H}$. If $E = 0$, (A 8*a*,*b*) reduce to their counterparts, (2.22*b*) and (2.23*a*), in the original model. To estimate E, we require the fluxes within the fountain at the upper interface. Kaye & Hunt (2006) identified three distinct classes of fountain behaviour, each with a different rise height dependence on the source Froude number. In our problem, as the 'source' conditions (at $z = h_1$) of the fountain are time-varying, its behaviour within layer 1 is complex. Assuming the fountain is quasi-steady at each time instance, we invoke a simplified model for its development through layer 1 based on the plume theory of Morton *et al.* (1956). Thus, for top-hat profiles, the equations for the conservation of volume flux Q_1, momentum flux M_1 and buoyancy flux $B_1' = B_1 - g_1'(t)Q_{11}(t) < 0$ of the fountain, take the form

$$\frac{\mathrm{d}Q_1}{\mathrm{d}z'} = 2\alpha_f\pi^{1/2}M_1^{1/2}, \quad \frac{\mathrm{d}M_1}{\mathrm{d}z'} = \frac{B_1'Q_1}{M_1}, \quad \frac{\mathrm{d}B_1'}{\mathrm{d}z'} = 0, \qquad \text{(A 9)}$$

where $\alpha_f = 0.085$ is the top-hat entrainment constant for a fountain (Kaye & Hunt 2006). Non-dimensionalizing (A 9) gives

$$\frac{\mathrm{d}q_1}{\mathrm{d}\hat{z}'} = \frac{5}{3}\frac{\alpha_f}{\alpha}m_1^{1/2}, \quad \frac{\mathrm{d}m_1}{\mathrm{d}\hat{z}'} = \frac{4}{3}\frac{f_1'q_1}{m_1}, \quad \frac{\mathrm{d}f_1'}{\mathrm{d}\hat{z}'} = 0, \qquad \text{(A 10)}$$

where $q_1 = Q_1/Q_{2,H}$, $m_1 = M_1/M_{2,H}$ and $f_1' = B_1'/B_2 = \psi - \psi^{1/3}\delta_1\xi_1^{5/3}$. When expressed in terms of the fluxes within the fountain at $\hat{z}' = \lambda_1$, namely Q_{12}, M_{12} and B_{12}, Fr_i takes the form

$$Fr_i = \frac{\pi^{1/4}M_{12}^{5/4}}{Q_{12}B_{12}^{1/2}} = \sqrt{\frac{5}{8\alpha}}\frac{m_{12}^{5/4}}{q_{12}f_{12}^{1/2}}, \qquad \text{(A 11)}$$

where $m_{12} = M_{12}/M_{2,H}$ and $f_{12} = B_{12}/B_{2,H} = (\delta_2 - \delta_1)q_{12}$.

https://doi.org/10.1017/jfm.2013.579 Published online by Cambridge University Press

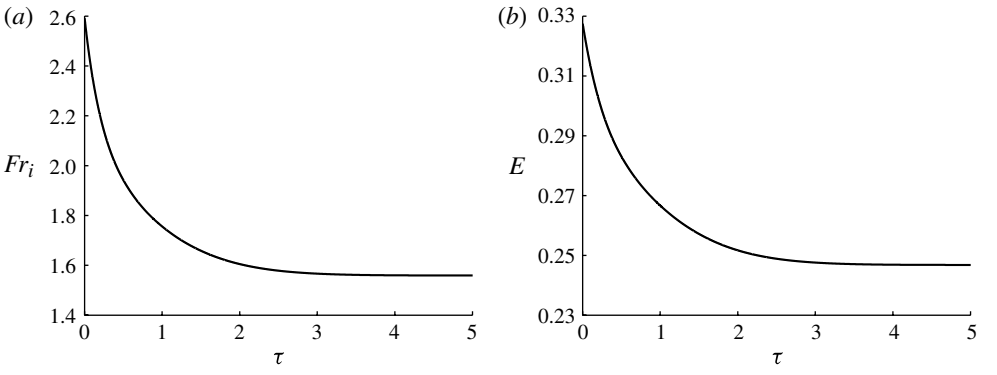


FIGURE 22. (*a*) Interfacial Froude number Fr_i and (*b*) entrainment flux E as functions of τ for $A = 0.5$ and $\psi = 0.3$.

The governing equations (2.22*a*), (2.23*b*) and (A 8*a*,*b*) were solved subject to the initial conditions prescribed in § 2.1 using a fourth-order Runge–Kutta finite-difference scheme. At each time instant, numerical solutions to the fountain equations (A 10), subject to the source conditions $(q_1(\hat{z}' = 0) = \psi^{1/3}\xi_1^{5/3}, m_1(\hat{z}' = 0) = \psi^{2/3}\xi_1^{4/3}, f_1'(\hat{z}' = 0) = f_1')$, were obtained to estimate Fr_i and E.

A.2.1. *Comparison of $E = 0$ and $E \neq 0$ models*

Figure 21 shows the two interface positions (*a*) and mean buoyancies (*b*) as functions of τ for an ascending flow when $A = 0.5$ and $\psi = 0.3$. The predictions of ξ_1 and δ_2 with $(E \neq 0)$ and without $(E = 0)$ fountain-top entrainment are in close agreement. Although the upper interface rises higher from its initial position when $E \neq 0$ than when $E = 0$, the differences between the two models in the predictions of ξ_2 are relatively small (less than 7 %).

Figures 22(*a*) and 22(*b*) reveal that Fr_i and E decrease with time. Given that λ_1 increases with τ (figure 6*a*), the fountain rises a greater distance before impingement on the upper interface at $\hat{z}' = \lambda_1$. Consequently, w_i decreases, whereas r_i increases, resulting in $Fr_i \propto w_i/\sqrt{r_i}$ decreasing with τ. Therefore, interfacial mixing is likely to be vigorous during the early transients.

REFERENCES

BAINES, W. D. 1975 Entrainment by a plume or jet at a density interface. *J. Fluid Mech.* **68**, 309–320.

BAINES, W. D. & TURNER, J. S. 1969 Turbulent buoyant convection from a source in a confined region. *J. Fluid Mech.* **37**, 51–80.

BARNETT, J. S. 1991 The dynamics of buoyant releases in confined spaces. PhD thesis, DAMTP, University of Cambridge.

BOWER, D. J., CAULFIELD, C. P., FITZGERALD, S. D. & WOODS, A. W. 2008 Transient ventilation dynamics following a change in strength of a point source of heat. *J. Fluid Mech.* **614**, 15–37.

COOMARASWAMY, I. A. & CAULFIELD, C. P. 2011 Time-dependent ventilation flows driven by opposing wind and buoyancy. *J. Fluid Mech.* **672**, 33–59.

COOPER, P. & LINDEN, P. F. 1996 Natural ventilation of an enclosure containing two buoyancy sources. *J. Fluid Mech.* **311**, 153–176.

ECONOMIDOU, M. & HUNT, G. R. 2010 Transient flows in enclosures: a generalized approach for modelling the effects of geometry, heat gains and wind. *Build. Environ.* **45**, 2607–2619.

https://doi.org/10.1017/jfm.2013.579 Published online by Cambridge University Press

FLYNN, M. R. & CAULFIELD, C. P. 2006 Natural ventilation in interconnected chambers. *J. Fluid Mech.* **564**, 139–158.

HOLFORD, J. M. & WOODS, A. W. 2007 On the thermal buffering of naturally ventilated buildings through internal thermal mass. *J. Fluid Mech.* **580**, 3–29.

HUGHES, G. O. & GRIFFITHS, R. W. 2008 Horizontal convection. *Annu. Rev. Fluid Mech.* **40**, 185–208.

HUNT, G. R. & COFFEY, C. J. 2010 Emptying boxes – classifying transient natural ventilation flows. *J. Fluid Mech.* **646**, 137–168.

HUNT, G. R. & LINDEN, P. F. 1998 Time-dependent displacement ventilation caused by variations in internal heat gains: application to a lecture theatre. In *Proc. ROOMVENT '98, the 6th Intl Conf. on Air Distribution in Rooms, Stockholm, Sweden* (ed. E. Mundt & T. G. Malmstrom), pp. 203–210. KTH Stockholm.

HUNT, G. R. & LINDEN, P. F. 2001 Steady-state flows in an enclosure ventilated by buoyancy forces assisted by wind. *J. Fluid Mech.* **426**, 355–386.

KAYE, N. B. & HUNT, G. R. 2004 Time-dependent flows in an emptying filling box. *J. Fluid Mech.* **520**, 135–156.

KAYE, N. B. & HUNT, G. R. 2006 Weak fountains. *J. Fluid Mech.* **558**, 319–328.

KAYE, N. B. & HUNT, G. R. 2007 Overturning in a filling box. *J. Fluid Mech.* **576**, 297–323.

KUMAGAI, M. 1984 Turbulent buoyant convection from a source in a confined two-layered region. *J. Fluid Mech.* **147**, 105–131.

LANE-SERFF, G. F. & SANDBACH, S. D. 2012 Emptying non-adiabatic filling boxes: the effects of heat transfers on the fluid dynamics of natural ventilation. *J. Fluid Mech.* **701**, 386–406.

LIN, Y. J. P. & LINDEN, P. F. 2005 The entrainment due to a turbulent fountain at a density interface. *J. Fluid Mech.* **542**, 25–52.

LINDEN, P. F. & COOPER, P. 1996 Multiple sources of buoyancy in a naturally ventilated enclosure. *J. Fluid Mech.* **311**, 177–192.

LINDEN, P. F., LANE-SERFF, G. F. & SMEED, D. A. 1990 Emptying filling boxes: the fluid mechanics of natural ventilation. *J. Fluid Mech.* **212**, 309–335.

MORTON, B. R., TAYLOR, G. & TURNER, J. S. 1956 Turbulent buoyant convection from a source in a confined region. *Proc. R. Soc. Lond.* A **234**, 1–23.

SCASE, M. M., CAULFIELD, C. P., DALZIEL, S. B. & HUNT, J. C. R. 2006 Time-dependent plumes and jets with decreasing source strengths. *J. Fluid Mech.* **563**, 443–461.

TURNER, J. S. 1986 Turbulent entrainment: the development of the entrainment assumption, and its application to geophysical flows. *J. Fluid Mech.* **173**, 431–471.

WAGNER, A., KLEBE, M. & PARKER, C. 2007 Monitoring results of a naturally ventilated and passively cooled office building in Frankfurt, Germany. *Intl J. Ventilation* **6**, 3–20.

WONG, A. B. D. & GRIFFITHS, R. W. 1999 Stratification and convection produced by multiple turbulent plumes. *Dyn. Atmos. Oceans* **30**, 101–123.

WONG, A. B. D., GRIFFITHS, R. W. & HUGHES, G. O. 2001 Shear layers driven by turbulent plumes. *J. Fluid Mech.* **434**, 209–241.

https://doi.org/10.1017/jfm.2013.579 Published online by Cambridge University Press